

STACKED RESIDUALS OF DYNAMIC LAYERS FOR TIME SERIES ANOMALY DETECTION

Luca Zancato

Department of Information Engineering
University of Padova
luca.zancato@phd.unipd.it

Alessandro Achille

Amazon Web Services
aachille@amazon.com

Giovanni Paolini

Amazon Web Services
paoling@amazon.com

Alessandro Chiuso

Department of Information Engineering
University of Padova
chiuso@dei.unipd.it

Stefano Soatto

Amazon Web Services
soattos@amazon.com

ABSTRACT

We present an end-to-end differentiable neural network architecture to perform anomaly detection in multivariate time series by incorporating a Sequential Probability Ratio Test on the prediction residual. The architecture is a cascade of dynamical systems designed to separate linearly predictable components of the signal such as trends and seasonality, from the non-linear ones. The former are modeled by local Linear Dynamic Layers, and their residual is fed to a generic Temporal Convolutional Network that also aggregates global statistics from different time series as context for the local predictions of each one. The last layer implements the anomaly detector, which exploits the temporal structure of the prediction residuals to detect both isolated point anomalies and set-point changes. It is based on a novel application of the classic CUMSUM algorithm, adapted through the use of a variational approximation of f -divergences. The model automatically adapts to the time scales of the observed signals. It approximates a SARIMA model at the get-go, and auto-tunes to the statistics of the signal and its covariats, without the need for supervision, as more data is observed. The resulting system, which we call STRIC, outperforms both state-of-the-art robust statistical methods and deep neural network architectures on multiple anomaly detection benchmarks.

1 INTRODUCTION

Time series data are being generated in increasing volumes in industrial, medical, commercial and scientific applications. Such growth is fueling demand for unsupervised anomaly detection algorithms (Munir et al., 2019; Geiger et al., 2020; Su et al., 2019). In large-scale applications, a number of time series often exhibit trends and seasonal changes over different time intervals from hourly to yearly. In addition to such “simple” phenomena, there may be complex correlations both within and across time series that must be captured in order to determine that an anomaly has occurred. While recent developments have focused on powerful deep neural network (DNN) architectures, especially Transformers (Xu et al., 2021), simple linear models are still preferred where dataset-specific tuning is impractical (Braei & Wagner, 2020) and interpretability of failure modes is desired (Geiger et al., 2020; Su et al., 2019). While powerful, general DNNs, and Transformers in particular, do not natively possess the inductive biases that are beneficial for modeling time series.

We introduce a novel architecture where each layer is a dynamical system. Just like convolutional layers are a particular subset of fully connected ones designed to capture locality as an inductive bias,

our Dynamic Layers are subsets of convolutional ones designed to capture causality as an inductive bias: the output sequence of each layer at a given time only depends on past values of the input sequence. To explicitly capture trends and seasonal components, thus improving interpretability, early Dynamic Layers model *linearly predictable* phenomena, and pass on their prediction residual to global non-linear Dynamic Layers. To train our architecture, we design a novel fading memory regularizer that allows the model to consider large intervals of past data (larger than the time scales of the underlying processes) and automatically selects the relevant past to avoid overfitting. The optimal estimated scale provides users with valuable insights on the characteristic temporal scales of the data.

The resulting model, which we call STRIC: Stacked Residuals of Dynamic Layers, is differentiable and trained end-to-end with a predictive loss. At inference time, the prediction residual is used in a sequential probability ratio test (SPRT) in order to detect anomalies Basseville & Nikiforov (1993). The SPRT we use is based on the classic CUMSUM algorithm, but modified to avoid estimating the distribution of residuals, otherwise required to compute the cumulative test statistics. Instead, we directly estimate the likelihood ratios with a variational characterization of f -divergences by solving a convex risk minimization problem in closed form.

STRIC differs from prior work in the architecture (design of Dynamic Layers, Section 4), in the regularization (fading memory, Section 4.1), and in the decision function (non-parametric SPRT, Section 5). These developments allow STRIC to couple the robustness of simple linear models with the flexibility of non-linear ones. At the same time, STRIC is not affected by the drawbacks of generic non-linear models, such as their tendency to overfit and their fragility to covariate shift. Summarizing, our main contributions are:

1. A novel stacked residual architecture with interpretable components that is naturally hierarchical and trained end-to-end: The first Linear Dynamic Layer (LDL) models trends, the second LDL models quasi-periodicity/seasonality at multiple temporal scales, the third LDL is a general linear predictor, and the fourth is a non-linear Dynamic Layer in the form of a Temporal Convolution Network (TCN). While the first three layers are *local* to each component of the time series, the last integrates *global* statistics across different time series (covariates). Our design of LDLs does not involve an explicit state-space model Haarnoja et al. (2017); Tíño (2019), and instead efficiently projects the input time series onto a basis of the spectral representation of the space of linear dynamical systems.
2. A novel regularization scheme for the prediction loss which allows automatic complexity selection according to the Empirical Bayes framework (Rasmussen & Williams, 2006). Learning entails back-propagating through a convex optimization (Amos & Kolter, 2017; Lee et al., 2019) which induces fading memory in the TCN, incentivizing LDLs to model long-term local statistics and leaving the task of modeling global residual correlations to the TCN.
3. A novel non-parametric extension of the CUMSUM algorithm which enables its use without having to estimate the distribution of residuals and without the need to introduce unrealistic modeling/dataset-specific assumptions. To the best of our knowledge, STRIC is the only deep learning-based method that forgoes a linear classifier rule in favor of CUMSUM.

2 RELATED WORK

A *time series* is an ordered sequence of data points. We focus on discrete and regularly spaced time indices, and thus we do not include literature specific to asynchronous time processes in our review. Categorizing by discriminant function, unsupervised anomaly detection paradigms roughly include: density-estimation, clustering-based and reconstruction-based methods.

Density-estimation methods exploit an estimate of the local density and local connectivity as a discriminant function: the anomaly score of each datum is measured by the degree of isolation from the surrounding data (Breunig et al., 2000). Clustering-based methods instead build clusters of normal data and the anomaly score of an instance is computed as the distance to the nearest cluster center (Zolhavarieh et al., 2014; Yeh et al., 2016; Shen et al., 2020). Reconstruction-based methods detect anomalies based on the reconstruction error of a “normal” model of the time series. In these methods it is common to use statistics of the prediction error as the discriminant (Braei & Wagner, 2020),

and in particular test the likelihood ratio between the distribution of the prediction error before and after a given time instant, to determine if that instant corresponds to an anomaly (Yashchin, 1993). Recent methods use deep neural network architectures and the Euclidean distance among activation vectors as a discriminant (Munir et al., 2019; Geiger et al., 2020; Su et al., 2019; Bashar & Nayak, 2020).

STRIC falls into the class of reconstruction-based methods, to which it contributes in two ways by introducing: (i) an architecture to compute the prediction residual, based on a novel Dynamic Layer design, and (ii) a novel decision function that extends the classic CUMSUM algorithm Basseville & Nikiforov (1993) to operate without explicit knowledge of the residual distribution. As a result of these design choices, STRIC is *interpretable*: it explicitly models trends and seasonality without reducing the representation power of the overall model; it is *flexible*, in the sense of being intrinsically multi-scale and auto-tuning. Specifically, at initialization, STRIC implements a multi-scale SARIMA model (Adhikari & Agrawal, 2013), which can function out-of-the-box on a wide variety of time series. As more data is observed, including from covariate time series, the model adapts without the need for supervision, in an end-to-end fashion.

Munir et al. (2019) argue that anomaly detection can be solved by exploiting a flexible model such as TCN, with a proper inductive bias. However, in Appendix A.8.1 we show that a TCN alone can overfit simple time series. We therefore focus on providing the architecture with temporal ordering as an explicit inductive bias, like (Bai et al., 2018; Sen et al., 2019; Tsang et al., 2018; Guen et al., 2020). However, unlike prior work, our temporal model has hierarchical structure (Oreshkin et al., 2019) and performs regularization *not* by maintaining an explicit finite-dimensional state, but by enforcing fading memory (Zancato & Chiuso, 2021) while retaining the information that is needed to predict future values.

3 NOTATION

We denote vectors with lower case and matrices with upper case. In particular y is a multi-variate time series $\{y(t)\}_{t \in \mathbb{Z}}$, $y(t) \in \mathbb{R}^n$; we stack observations from time t to $t + k - 1$ and denote the resulting matrix as $Y_t^{t+k-1} := [y(t), y(t+1), \dots, y(t+k-1)] \in \mathbb{R}^{n \times k}$. We denote the i -th component of y as y_i and its value at time t as $y_i(t) \in \mathbb{R}$. We refer to intervals in $\{y(s), s > t\}$ as future/test and those in $\{y(s), s \leq t\}$ as past/reference. At time t , sub-sequences containing the n_p past samples up to time $t - n_p + 1$ are given by $Y_{t-n_p+1}^t$ (note that we include the present data into the past data), while future samples up to time $t + n_f$ are $Y_{t+1}^{t+n_f}$. We will use past data to predict future ones, where the length of past and future intervals are design hyper-parameters.

4 TEMPORAL RESIDUAL ARCHITECTURE

We now describe STRIC’s main design principles. Each block maps sequence-to-sequence causally, *i.e.*, its output at a given time only depends on its past inputs. This could be done by “unrolling” a state-space model (Haarnoja et al., 2017; Tiño, 2019), where the state encodes the memory of past data. This is ineffective as distant memories are diluted in the state update and training becomes difficult Hochreiter & Schmidhuber (1997). We follow (Bai et al., 2018) and instead use causal convolutions with a fixed-size 1-D kernel to capture long range dependencies. However, both our architecture, depicted in Figure 1, and the training procedure, which we describe next, differ from prior work.

Linear Dynamic Layer. Rather than an explicit state space, or a fixed convolution kernels, we model linear dynamics using a large but fixed set of randomly chosen (marginally) stable finite dimensional impulse responses (Farahmand et al., 2017). In particular the first linear dynamic layer models and removes slow-varying components in the input data. We initialize the filters to mimic a causal Hodrick Prescott filter (Ravn & Uhlig, 2002) with poles close to one. The second linear dynamic layer models and removes periodic components: it is initialized with poles on the unit circle (periodic impulse response). Finally, the third layer implements a linear stationary filter bank whose impulse response has poles in the complementary region within the unit circle relative to previous linear layers. See Appendix A.1 for more details regarding the initialization strategy and the residual connections.

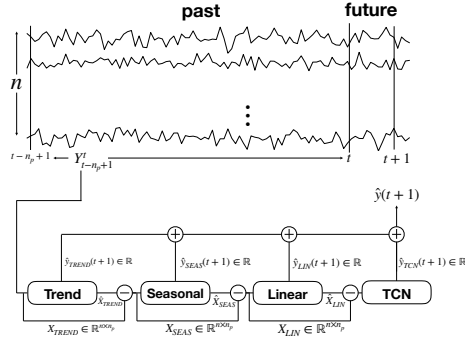
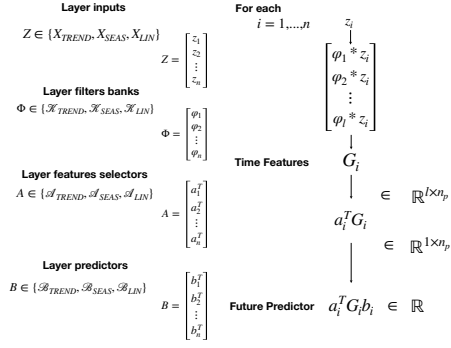


Figure 1: STRIC predictor architecture.

Figure 2: **Linear Dynamic Layers.** Time features are extracted independently for each time series (see Appendix A.1 for more details).

Non-linear Dynamic Layer. The *Non-linear Dynamic Layer* module aggregates global statistics from different time series using a TCN model (Sen et al., 2019). It takes as input the prediction residual of the linear layers and outputs a matrix $G(Y_{t-n_p+1}^t) \in \mathbb{R}^{l \times n_p}$ where l is the number of output features extracted by the TCN model. The column $G(Y_{t-n_p+1}^t)_j$ with $j = 1, \dots, n_p$ of the non-linear features is computed using data up to time $t - n_p + j$ thanks to the causal internal structure of a TCN network (Bai et al., 2018). We build a linear predictor on top of $G(Y_{t-n_p+1}^t)$ for each single time series independently: the predictor of the i -th time series is given by: $\hat{y}_{\text{TCN}}(t+1)_i := a_i^T G(Y_{t-n_p+1}^t) b_i$ where $a_i \in \mathbb{R}^l$ and $b_i \in \mathbb{R}^{n_p}$. Since a_i combines features (uniformly in time) we can interpret it as a feature selector. While b_i aggregates relevant features across time indices to build the one-step ahead predictor (see Appendix A.1 for further details). As anticipated, this is a superset model of the preceding layers, making the overall architecture redundant. Therefore, we introduce a novel regularization which incentivizes the Non-linear Dynamic Layer to model the most recent past of the global residuals and leaves LDLs to model long term local statistics.

4.1 AUTOMATIC COMPLEXITY DETERMINATION

Let the TCN-based future predictor be $\hat{y}_{\text{TCN}}(t+1) := a^T G(Y_{t-n_p+1}^t) b = \hat{X}_{\text{TCN}} b$ where $\hat{X}_{\text{TCN}} \in \mathbb{R}^{1 \times n_p}$ is the output of the TCN block which depends on the past window $Y_{t-n_p+1}^t$ of length n_p (the memory of the predictor).¹ Ideally, n_p should be large enough to capture the “true” memory of the time series, but should not be too large if not necessary, according to the desired bias variance trade-off. In this section, we introduce a novel regularized loss inspired by Bayesian arguments which allows us to use an architecture with a “large enough” past horizon n_p (larger than the true system memory) and automatically select the *relevant past* to avoid overfitting. Such information is exposed to the user through an interpretable parameter λ that directly measures the *relevant time scale* of the signal.

Bayesian learning formulation: The ideal model would yield an innovation process (residual prediction error) that is white and Normal. Accordingly, $y(t+1) | Y_{t-n_p+1}^t \sim \mathcal{N}(F^*(Y_{t-n_p+1}^t), \eta^2)$ where F^* is the optimal predictor of the future values given the past. Note that this modeling assumption does not restrict our framework and is used only to justify the use of the squared loss to learn the regression function of the predictor. In practice, we do not know F^* and we approximate it with our parametric predictor. For ease of exposition, we group all architecture parameters except b in W (linear filters parameters, TCN kernel parameters etc.) and write the conditional likelihood of the future given the past data of our predictor as $p(Y_{t+1}^{t+n_f} | b, W, Y_{t-n_p+1}^t) = \prod_{k=1}^{n_f} p(y(t+k) | b, W, Y_{t+k-n_p}^{t+k-1})$.

To simplify, we call $Y_f := Y_{t+1}^{t+n_f} \in \mathbb{R}^{n_f}$ the set of future outputs over which the predictor is computed and $\hat{Y}_{b,W} \in \mathbb{R}^{n_f}$ the predictor’s outputs.

¹For simplicity of notation, we describe scalar time series, leaving the multivariate case to (Appendix A.2.2).

The optimal set of parameters can be found by maximizing the posterior $p(b, W | Y_f)$ over the model parameters. We model b and W as independent random variables:

$$p(b, W | Y_f) \propto p(Y_f | b, W)p(b)p(W) \quad (1)$$

where $p(b)$ is the prior associated to the predictor coefficients and $p(W)$ is the prior on the remaining parameters. The prior $p(b)$ should encode our belief that the prediction model should not be too complex and should depend only on the *most relevant past*. We model this by assuming that the components of b have zero mean and exponentially decaying variances: $\mathbb{E}b_{n_p-j-1}^2 = \kappa\lambda^j$ for $j = 0, \dots, n_p - 1$, where $\kappa \in \mathbb{R}^+$ and $\lambda \in (0, 1)$. Under such constraints the maximum entropy prior $p_{\lambda, \kappa}(b)$ (Cover & Thomas, 1991) is $\log(p_{\lambda, \kappa}(b)) \propto -\|b\|_{\Lambda^{-1}}^2 - \log(|\Lambda|)$ where $\Lambda \in \mathbb{R}^{n_p}$ is a diagonal matrix with elements $\Lambda_{j,j} = \kappa\lambda^j$ with $j = 0, \dots, n_p - 1$. Here, λ represents how fast the output of the predictor “forgets” the past. Therefore, λ regulates the complexity of the predictor: the smaller λ , the lower the complexity.

In practice, λ has to be estimated from the data. One would be tempted to estimate jointly b, W, λ, κ (and possibly η) by minimizing the negative log of the joint posterior (see Appendix A.2.1). Unfortunately, this leads to a degeneracy since the joint negative log posterior goes to $-\infty$ when $\lambda \rightarrow 0$. Indeed, typically the parameters describing the prior (such as λ) are estimated by maximizing the marginal likelihood, i.e., the likelihood of the data once the parameters (b, W) have been integrated out. Since computing (or even approximating) the marginal likelihood in this setup is prohibitive, we now introduce a variational upper bound to the marginal likelihood which is easier to estimate.

Variational upper bound to the marginal likelihood: The model structure we consider is linear in b and we can therefore stack the predictions of each available time index t to get the following linear predictor on the whole future data: $\hat{Y}_{b,W} = F_W b$ where $F \in \mathbb{R}^{n_f \times n_p}$ is obtained by stacking $\hat{X}_{\text{TCN}}(Y_{i-n_p+1}^i)$ for $i = t, \dots, t + n_f - 1$.

Proposition 4.1 Consider a model on the form: $\hat{Y}_{b,W} = F_W b$ (linear in b and possibly non-linear in W) and its posterior in Equation (1). Assume the prior on the parameters b is given by the maximum entropy prior and W is fixed. Then the following is an upper bound on the marginal likelihood associated to the posterior in Equation (1) with marginalization taken only w.r.t. b :

$$\mathcal{U}_{b,W,\Lambda} = \frac{1}{\eta^2} \left\| Y_f - \hat{Y}_{b,W} \right\|^2 + b^\top \Lambda^{-1} b + \log \det(F_W \Lambda F_W^\top + \eta^2 I)$$

This regularized loss (proved in Appendix A.2) provides an alternative loss function to the negative log posterior which does not suffer from the degeneracy above while allowing optimization over b, W, λ and κ . For that, we shall use Equation (2) as a regularized reconstruction loss to learn our predictive model and automatically find the optimal *time scale* λ .

Remark: We use batch normalization (Ioffe & Szegedy, 2015) along the rows of F_W so that features have comparable scales; this avoids the TCN network countering the fading regularization by increasing its output scales (see Appendix A.2.3).

The STRIC model represents a parametric function class trained to produce the prediction residual in response to an input time series. In the next section, we describe how to use such a residual to detect anomalies.

5 ANOMALY SCORE ON PREDICTION RESIDUALS

Our method to compute anomaly scores is based on a variational approximation of the likelihood ratio between two windows of prediction residuals. We use the prediction residuals of our residual architecture to test the hypothesis that the time instant t is anomalous by comparing its statistics before t on temporal windows of length n_n and n_a . The detector is based on the likelihood ratios aggregated sequentially using the classical CUMSUM algorithm (Page, 1954; Yashchin, 1993). CUMSUM, however, requires knowledge of the distributions, which we do not have. Unfortunately, the problem of estimating the densities is hard (Vapnik, 1998) and generally intractable for high-dimensional time series (Liu et al., 2012). We circumvent this problem by directly estimating the likelihood ratio with a variational characterization of f -divergences (Nguyen et al., 2010) which

Table 1: **Comparison with SOTA anomaly detectors:** We compare STRIC with other anomaly detection methods (see Appendix A.9) on the experimental setup and the same evaluation metrics proposed in Lai et al. (2021); Xu et al. (2021). The baseline models are: VAR, OCSVM (Schölkopf et al., 2000), IForest (Liu et al., 2008), DAGMM (Zong et al., 2018), LSTM (Braei & Wagner, 2020; Munir et al., 2019), OmniAnomaly (Su et al., 2019), THOC (Shen et al., 2020), Anomaly Transformer (Xu et al., 2021).

F1 - multivariate datasets		Credit Card	CICIDS	GECCO	SWAN-SF	SMD	PSM
Models	VAR	0.192	0.030	0.349	0.385	0.741	0.871
	OCSVM	0.183	0.007	0.296	0.485	0.562	0.707
	IForest	0.168	0.016	0.391	0.583	0.536	0.835
	DAGMM	0.062	0.013	0.074	0.271	0.709	0.808
	LSTM	0.007	0.046	0.305	0.312	0.828	0.810
	OmniAnomaly	0.084	0.049	0.330	0.405	0.886	0.808
	THOC					0.850	0.895
	Anomaly Transformer					0.923	0.979
	STRIC (ours)	0.203	0.051	0.418	0.669	0.926	0.979

involves solving a convex risk minimization problem in closed form. The overall method is entirely unsupervised, and users can tune the scale parameter (corresponding to the window of observation when computing the likelihood ratios) and the coefficient of CUMSUM depending on the application and desired operating point in the tradeoff between missed detection and false alarms.

5.1 LIKELIHOOD RATIOS AND CUMSUM

CUMSUM (Page, 1954) is a classical Sequential Probability Ratio Test (SPRT) (Basseville & Nikiforov, 1993; Liu et al., 2012) of the null hypothesis H_0 that the data after the given time c comes from the same distribution as before, against the alternative hypothesis H_c that the distribution is different. We denote the distribution before c as p_n and the distribution after the anomaly at time c as p_a . If the density functions p_n and p_a were known (we shall relax this assumption later), the optimal statistic to decide whether a datum $y(i)$ is more likely to come from one or the other is the likelihood ratio $s(y(i))$. According to the Neyman-Pearson lemma, H_0 is accepted if the likelihood ratio $s(y(i))$ is less than a threshold chosen by the operator, otherwise H_c is chosen. In our case, the competing hypotheses are $H_0 = \text{“no anomaly has happened”}$ and $H_c = \text{“an anomaly happened at time } c\text{”}$. We denote with p_{H_0} and p_{H_c} the p.d.f.s under H_0 and H_c so that: $p_{H_0}(Y_1^K) = p_n(Y_1^K)$ and $p_{H_c}(Y_1^{c-1}) = p_n(Y_1^{c-1})$, $p_{H_c}(Y_c^K | Y_1^{c-1}) = p_a(Y_c^K | Y_1^{c-1})$. Therefore the likelihood ratio is:

$$\Omega_c^t := \frac{p_{H_c}(Y_1^t)}{p_{H_0}(Y_1^t)} = \frac{p_n(Y_1^{c-1})p_a(Y_c^t | Y_1^{c-1})}{p_n(Y_1^t)} = \frac{p_a(Y_c^t | Y_1^{c-1})}{p_n(Y_c^t | Y_1^{c-1})} = \prod_{i=c}^t \frac{p_a(y(i) | Y_1^{i-1})}{p_n(y(i) | Y_1^{i-1})} \quad (2)$$

To determine the presence of an anomaly, we can compute the cumulative sum $S_c^t := \log \Omega_c^t$ of the log likelihood ratios, which depends on the time c , and estimate the true change point c^* using a maximum likelihood criterion, corresponding to the detection function $h_t = \max_{1 \leq c \leq t} S_c^t$. The first instant at which we can confidently assess the presence of a change point (a.k.a. stopping time) is: $c_{\text{stop}} = \min\{t : h_t \geq \epsilon\}$ where ϵ is a design parameter that modulates the sensitivity of the detector depending on the application. The final estimate \hat{c} of the true change point after the detection c_{stop} is given by the timestamp c at which $h_{c_{\text{stop}}} = \max_{1 \leq c \leq c_{\text{stop}}} S_c^{c_{\text{stop}}}$ is achieved. In Appendix A.3, we provide an alternative derivation that shows that CUMSUM is a comparison of the test statistic with an adaptive threshold that keeps complete memory of past ratios. The next step is to relax the assumption of known densities, which we bypass in the next section by directly approximating the likelihood ratios to compute the cumulative sum.

5.1.1 LIKELIHOOD RATIO ESTIMATION WITH PEARSON DIVERGENCE

The goal of this section is to tackle the problem of estimating the likelihood ratio of two general distributions p_n and p_a given samples. To do so, we leverage a variational approximation of f -divergences (Nguyen et al., 2010) whose optimal solution is directly connected to the likelihood

ratio. For different choices of divergence function, different estimators of the likelihood ratio can be built. We focus on a particular divergence choice, the Pearson divergence, since it provides a closed form estimate of the likelihood ratio (see Appendix A.4).

Proposition 5.1 (Nguyen et al., 2010; Liu et al., 2012) *Let $\phi := p_a/p_n$ be the likelihood ratio of the unknown distributions p_a and p_n . Let $\mathcal{F} := \{f_i : f_i \sim p_a, i = 1, \dots, n_a\}$ and $\mathcal{H} := \{h_i : h_i \sim p_n, i = 1, \dots, n_n\}$ be two sets containing n_a and n_n samples i.i.d. from p_a and p_n respectively. An empirical estimator $\hat{\phi}$ of the likelihood ratio ϕ is given by the solution to the following convex optimization problem:*

$$\hat{\phi} = \arg \min_{\phi} \frac{1}{2n_n} \sum_{i=1}^{n_n} \phi(h_i)^2 - \frac{1}{n_a} \sum_{i=1}^{n_a} \phi(f_i) \quad (3)$$

Proposition 5.2 (Liu et al., 2012; Kanamori et al., 2009) *Let ϕ in Equation (3) be chosen in the family of Reproducing Kernel Hilbert Space (RKHS) functions Φ induced by the kernel k . Let the kernel sections be centered on the set of data $\mathcal{S}_{tr} := \{\mathcal{F}, \mathcal{H}\}$ and let the kernel matrices evaluated on the data from p_a and p_n be $K_a := K(\mathcal{F}, \mathcal{S}_{tr})$ and $K_n := K(\mathcal{H}, \mathcal{S}_{tr})$. The optimal regularized empirical likelihood ratio estimator on a new datum e is given by:*

$$\hat{\phi}(e) = \frac{n_n}{n_a} K(e, \mathcal{S}_{tr}) \left(K_n^T K_n + \gamma n_n I_{n_n+n_a} \right)^{-1} K_a^T \mathbb{1} \quad (4)$$

Remark: The estimator in Equation (4) is not constrained to be positive. Nonetheless, the positivity constraints can be enforced. In this case, the closed form solution is no longer valid but the problem remains convex.

5.2 SUBSPACE LIKELIHOOD RATIO ESTIMATION AND CUMSUM

We now present our novel anomaly detector estimator. We test for an anomaly in the data Y_1^t by looking at the prediction residuals E_1^t obtained from our time series predictor of the normal behaviour, which is a sufficient representation of Y_1^t (see Appendix A.5). This guarantees that the sequence E_1^t is white in each of its normal subsequences. On the other hand, if the model is applied to a data subsequence which contains an abnormal condition, the residuals are correlated.

We estimate the likelihood ratio of p_a and p_n on a datum e_t as $\hat{\phi}_t(e_t)$. $\hat{\phi}_t$ is obtained by applying Equation (4) on the past window of size $n_n + n_a$. At each time instant t , we compute the necessary kernel matrices as $K_a(E_{t-n_a+1}^t, E_{t-n_n-n_a+1}^t)$ and $K_n(E_{t-n_n-n_a+1}^t, E_{t-n_n-n_a+1}^t)$.

Algorithm 1 Non-parametric CUMSUM

Require: Sequence of prediction residuals e_i with $i \in \{0, \dots, T\}$, kernel function k , pre-anomaly and post-anomaly reference window lengths n_n and n_a , CUMSUM threshold ϵ .

```

1:  $\hat{S}_0^{n_n+n_a-1} \leftarrow 0$  {Initialize cumulative sum}
2: for  $t \in \{n_n + n_a, \dots, T\}$  do
3:    $E_n \leftarrow E_{t-n_n-n_a+1}^t, E_a \leftarrow E_{t-n_a+1}^t$ 
4:    $K_p \leftarrow K(E_n, E_{t-n_n-n_a+1}^t)$ 
5:    $K_f \leftarrow K(E_a, E_{t-n_n-n_a+1}^t)$ 
6:   Compute likelihood ratio estimate  $\hat{\phi}_t(e_t)$  with Equation (4) {Estimate lik. ratio}
7:    $\hat{S}_0^t \leftarrow \hat{S}_0^{t-1} + \log \hat{\phi}_t(e_t)$  {Update cumulative sum}
8:    $m_t = \min_{1 \leq j \leq t} \hat{S}_0^j$  {Update minimum}
9:    $t_{\text{stop}} \leftarrow \min\{k : \hat{S}_0^k \geq m_k + \epsilon\}$ 
10:  if  $t_{\text{stop}} \neq \emptyset$  then
11:    return  $\arg \min_{1 \leq j \leq t_{\text{stop}}} \hat{S}_0^j$ 
12:  end if
13: end for

```

Remark: At time t , the likelihood ratio is estimated assuming i.i.d. data. This assumption holds if no anomaly happened but does not hold in the abnormal situation since residuals are not i.i.d. In

Table 2: **Ablation study on the RMSE of prediciton errors:** We compare Test error and Generalization Gap (Gap.) of a standard TCN model with our STRIC predictor and some variation of it (using the same training hyper-parameters).

	TCN		TCN + Linear		TCN + Fading		STRIC pred	
	Test	Gap.	Test	Gap.	Test	Gap.	Test	Gap.
Datasets								
Credit Card	0.83	0.78	0.52	0.25	0.54	0.23	0.44	0.15
CICIDS	0.94	0.68	0.86	0.57	0.78	0.31	0.50	0.09
GECCO	1.14	1.06	1.04	0.99	0.95	0.68	0.84	0.20
SWAN-SF	0.92	0.88	0.81	0.75	0.77	0.51	0.62	0.15
SMD	0.31	0.17	0.29	0.16	0.31	0.14	0.27	0.10
PSM	0.28	0.09	0.24	0.07	0.21	0.04	0.19	0.03

Appendix A.5, we prove that treating correlated variables as uncorrelated provides a lower bound on the actual cumulative sum of likelihood ratios. For a fixed threshold, this means the detector cumulates less and therefore requires more time to reach the threshold.

Finally, we compute the detector function by aggregating the estimated likelihood ratios: $\hat{S}_c^t := \sum_{i=c}^t \log \hat{\phi}_i(e_i)$.

Remark: The choice of the windows length (n_n and n_a) is fundamental and highly influences the likelihood estimator. Using small windows makes the detector highly sensible to point outliers, while larger windows are better suited to estimate sequential outliers (see Appendix A.5).

6 EXPERIMENTAL RESULTS

In this section, we show that STRIC can be successfully applied to detect anomalous behaviours on different anomaly detection benchmarks. In particular, we test our novel residual temporal structure, the automatic complexity regularization and the anomaly detector on the following multivariate datasets: Credit Card, CICIDS, GECCO, SWAN-SF (part of TODS, a multivariate anomaly detection benchmark (Lai et al., 2021)), SMD (Su et al., 2019) and PSM (Abdulaal et al., 2021). Descriptions and statistical details are summarized in Appendix A.6, see Appendix A.7 for the experimental setup and data normalization.

Anomaly detection: While recent works show deep learning models are not well suited to solve AD on standard anomaly detection benchmarks (Braei & Wagner, 2020; Lai et al., 2021), we prove deep models can be effective provided they are equipped with a proper inductive bias and regularization. In Table 1, we show that STRIC improves over the existing state-of-the-art anomaly detection methods, both classical (e.g. VAR/OCSVM/IForest) and deep learning based. Our experiments follow the experimental setup and evaluation criteria used in Lai et al. (2021) and Xu et al. (2021).

To begin with, note that classical anomaly detection algorithms outperform deep learning methods on half of the datasets we use Lai et al. (2021): Credit Card, GECCO, SWAN-SF. We further verify this observation on other typical anomaly detection benchmarks in the appendix: Table 5. The fact that STRIC is on par or better than classical anomaly detection algorithms on these datasets highlights the importance of the modelling biases we introduce on the predictor: linear dynamical layers and fading regularization. We further validate this in Appendix A.8.1 where we show that STRIC’s inductive biases easily allow modelling time series characterized by trend and seasonal components, while deep learning based methods fail.

STRIC remains competitive on datasets in which deep models prevail. On CICIDS it outperforms OmniAnomaly Su et al. (2019), a reconstruction-based method built on a stochastic recurrent neural network architecture and planar normalizing flows for computing reconstruction probabilities. Moreover, STRIC performs comparably to Anomaly Transformer on SMD and PSM (Xu et al., 2021). The authors of (Xu et al., 2021) propose to use association discrepancy and transformer architectures to improve pointwise reconstruction-based methods. Our results suggest that using our non-parametric CUMSUM anomaly classifier which aggregates information over time, opposed to pointwise thresholding of the prediction residuals, leads to equally good results while allowing us to use an interpretable predictive model.

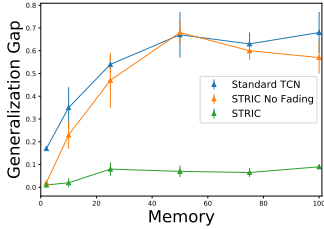


Figure 3: figure
Automatic complexity selection: Fading memory regularization preserves Generalization Gap as the memory of the predictor n_p increases on CICIDS.

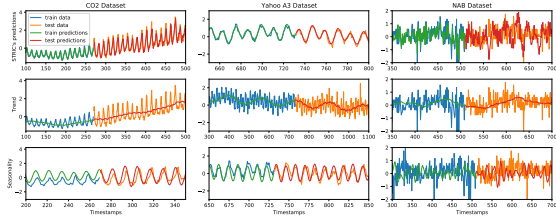


Figure 4: We test STRIC time series LDLs on different datasets (columns). In each panel, we show both training data and test data (see colors). **First row:** STRIC time series predictor (output of non-linear module). **Second row:** Trend components extracted by the LDLs. **Third row:** Seasonal components extracted by the LDLs.

STRIC interpretable time series decomposition: In Figure 4, we show STRIC’s interpretable decomposition on some toy and real world time series (see Appendix A.6 for details on these datasets). We report predicted signals (first row), estimated trends (second row) and seasonalities (third row) for different datasets. For all experiments, we plot both training data (first 40% of each time series) and test data. Note the interpretable components of STRIC generalize outside the training data, thus making STRIC work well on non-stationary time series (e.g. where the trend component is non-negligible and typical non-linear models overfit, see Appendix A.8.1).

Automatic complexity selection: In Figure 3, we test the effects of our automatic complexity selection (fading memory regularization) on STRIC. We compare STRIC with a standard TCN model and STRIC without regularization, as the memory of the predictor increases. The test error of STRIC is uniformly smaller than a standard TCN (without LDLs nor fading regularization). Adding LDLs to a standard TCN improves generalization for a fixed memory w.r.t. standard TCN but gets worse (overfitting occurs) as soon as the available past data horizon increases. On the other hand, the generalization gap of STRIC does not deteriorate as the memory of the predictor increases (see Appendix A.8 for a comparison with other metrics).

Ablation study: We now compare the prediction performance of a general TCN model with STRIC where we remove LDLs and fading regularization one at the time. In Table 2, we report the test RMSE prediction errors and the RMSE generalization gap (i.e. difference between test and training RMSE prediction errors) for different datasets while keeping the same training parameters (e.g. training epochs, learning rates etc.) and model parameters (e.g. $n_b = 100$). The addition of the linear interpretable model before the TCN slightly improves the test error for all datasets. We note this effect is more visible on Credit Card, GECCO and SWAN-SF: the datasets in which classical anomaly detection algorithms (including VAR) perform the best.

While the generalization of STRIC is always better than that of a standard TCN model or ablated STRIC, we note that applying fading memory regularization alone to a standard TCN does not always improve generalization (but never decreases it): this highlights that the benefits of combining the linear module and the fading regularization together are not a trivial ‘sum of the parts’. Consider for example SMD: STRIC achieves 0.27 test error, the best ablated model (TCN + Linear) 0.29, while TCN + Fading does not improve over the baseline TCN. A similar observation holds for other datasets too, see Table 6. These results suggest that fading regularization alone might not be beneficial (nor detrimental) for time series containing purely periodic components, which correspond to infinite memory systems (systems with unitary fading coefficient), or when the length of predictor’s input windows is not large enough. In the first case, the interpretable module is essential in removing the periodicities and providing the regularized non-linear module (TCN + Fading) with a residual that is easier to model; however, in the latter case, there is no gain in constraining the non-linear layer to look only at a subset of the input window since all the available past is informative for prediction. To conclude, our proposed fading regularization has (on average) a beneficial effect in controlling the complexity of a standard TCN model and reduces its generalization gap ($\approx 35\%$ reduction). Moreover, coupling fading regularization with the interpretable module guarantees the best generalization.

In Appendix A.8, we show further studies on the effects of STRIC’s hyper-parameters on its performance. In particular, we find that STRIC is highly sensitive to the choice of the length of the windows (n_a and n_n) used to estimate the likelihood ratio, while being much more robust to the choice of the memory of the predictor. We leave for future work the optimal design of the horizon lengths n_a and n_n .

7 DISCUSSION AND CONCLUSIONS

Unlike purely DNN-based methods (Geiger et al., 2020; Munir et al., 2019; Bashar & Nayak, 2020), STRIC exposes to the user both an interpretable time series decomposition (Cleveland et al., 1990) and the relevant time scale of the time series. We find that both Linear Dynamical Layers and the fading memory regularization are important in building a successful model (see Table 2). In particular, LDLs helps STRIC generalize correctly on non-stationary time series on which standard deep models (such as TCNs) overfit (Braei & Wagner, 2020). Moreover, we show that our novel fading regularization can improve the generalization error of TCNs up to $\approx 35\%$ over standard TCNs, provided the periodic components of the time series are captured and the time horizon is not chosen too small (Section 6). We highlight that the overall computational complexity and memory requirement of our method remain the same as standard TCNs, so that STRIC can be easily deployed on large-scale time series datasets.

Making the non-parametric anomaly detector fully adaptive to the data is an interesting research direction: while our fading window regularizer automatically tunes the predictor’s window length by exploiting the self-supervised nature of the prediction task, methods to automatically tune the detector’s window lengths (an unsupervised problem) are worth further investigations. Moreover, designing statistically optimal rules to calibrate our detector’s threshold ϵ based on the desired operating point (a tradeoff between missed detection and false alarms) would further enhance the out-of-the-box robustness of our method.

REFERENCES

- Ahmed Abdulaal, Zhuanghua Liu, and Tomer Lancewicki. *Practical Approach to Asynchronous Multivariate Time Series Anomaly Detection and Localization*, pp. 2485–2494. Association for Computing Machinery, New York, NY, USA, 2021. ISBN 9781450383325. URL <https://doi.org/10.1145/3447548.3467174>.
- Ratnadip Adhikari and R. K. Agrawal. An introductory study on time series modeling and forecasting. *CoRR*, abs/1302.6613, 2013. URL <http://arxiv.org/abs/1302.6613>.
- Brandon Amos and J Zico Kolter. Optnet: Differentiable optimization as a layer in neural networks. In *International Conference on Machine Learning*, pp. 136–145. PMLR, 2017.
- Shaojie Bai, J Zico Kolter, and Vladlen Koltun. An empirical evaluation of generic convolutional and recurrent networks for sequence modeling. *arXiv preprint arXiv:1803.01271*, 2018.
- Md Abul Bashar and Richi Nayak. Tanogan: Time series anomaly detection with generative adversarial networks. In *2020 IEEE Symposium Series on Computational Intelligence (SSCI)*, pp. 1778–1785. IEEE, 2020.
- Michèle Basseville and Igor V. Nikiforov. *Detection of Abrupt Changes: Theory and Application*. Prentice-Hall, Inc., USA, 1993. ISBN 0131267809.
- Liron Bergman and Yedid Hoshen. Classification-based anomaly detection for general data. In *International Conference on Learning Representations*, 2020. URL https://openreview.net/forum?id=H11K_1BtvS.
- Ane Blázquez-García, Angel Conde, Usue Mori, and Jose A Lozano. A review on outlier/anomaly detection in time series data. *arXiv preprint arXiv:2002.04236*, 2020.
- Mohammad Braei and Sebastian Wagner. Anomaly detection in univariate time-series: A survey on the state-of-the-art. *CoRR*, abs/2004.00433, 2020. URL <https://arxiv.org/abs/2004.00433>.

- Markus M. Breunig, Hans-Peter Kriegel, Raymond T. Ng, and Jörg Sander. Lof: Identifying density-based local outliers. *SIGMOD Rec.*, 29(2):93–104, may 2000. ISSN 0163-5808. doi: 10.1145/335191.335388. URL <https://doi.org/10.1145/335191.335388>.
- Robert B. Cleveland, William S. Cleveland, Jean E. McRae, and Irma Terpenning. Stl: A seasonal-trend decomposition procedure based on loess (with discussion). *Journal of Official Statistics*, 6: 3–73, 1990.
- T. M. Cover and J. A. Thomas. *Elements of Information Theory*. Series in Telecommunications and Signal Processing. Wiley, 1991.
- Jacob Devlin, Ming-Wei Chang, Kenton Lee, and Kristina Toutanova. BERT: pre-training of deep bidirectional transformers for language understanding. In Jill Burstein, Christy Doran, and Tamar Solorio (eds.), *Proceedings of the 2019 Conference of the North American Chapter of the Association for Computational Linguistics: Human Language Technologies, NAACL-HLT 2019, Minneapolis, MN, USA, June 2-7, 2019, Volume 1 (Long and Short Papers)*, pp. 4171–4186. Association for Computational Linguistics, 2019. doi: 10.18653/v1/n19-1423. URL <https://doi.org/10.18653/v1/n19-1423>.
- Amir-massoud Farahmand, Sepideh Pourazarm, and Daniel Nikovski. Random projection filter bank for time series data. In I. Guyon, U. V. Luxburg, S. Bengio, H. Wallach, R. Fergus, S. Vishwanathan, and R. Garnett (eds.), *Advances in Neural Information Processing Systems*, volume 30. Curran Associates, Inc., 2017. URL <https://proceedings.neurips.cc/paper/2017/file/ca3ec598002d2e7662e2ef4bdd58278b-Paper.pdf>.
- Alexander Geiger, Dongyu Liu, Sarah Alnegheimish, Alfredo Cuesta-Infante, and Kalyan Veeramachaneni. Tadgan: Time series anomaly detection using generative adversarial networks. *arXiv preprint arXiv:2009.07769*, 2020.
- Vincent Le Guen, Yuan Yin, Jérémie Dona, Ibrahim Ayed, Emmanuel de Bézenac, Nicolas Thome, and Patrick Gallinari. Augmenting physical models with deep networks for complex dynamics forecasting. *arXiv preprint arXiv:2010.04456*, 2020.
- Tuomas Haarnoja, Anurag Ajay, Sergey Levine, and Pieter Abbeel. Backprop kf: Learning discriminative deterministic state estimators, 2017.
- Sepp Hochreiter and Jürgen Schmidhuber. Long Short-Term Memory. *Neural Computation*, 9(8):1735–1780, 11 1997. ISSN 0899-7667. doi: 10.1162/neco.1997.9.8.1735. URL <https://doi.org/10.1162/neco.1997.9.8.1735>.
- Sergey Ioffe and Christian Szegedy. Batch normalization: Accelerating deep network training by reducing internal covariate shift. *CoRR*, abs/1502.03167, 2015. URL <http://arxiv.org/abs/1502.03167>.
- Takafumi Kanamori, Shohei Hido, and Masashi Sugiyama. A least-squares approach to direct importance estimation. *Journal of Machine Learning Research*, 10(48):1391–1445, 2009. URL <http://jmlr.org/papers/v10/kanamori09a.html>.
- Kwei-Herng Lai, Daochen Zha, Junjie Xu, Yue Zhao, Guanchu Wang, and Xia Hu. Revisiting time series outlier detection: Definitions and benchmarks. In *Thirty-fifth Conference on Neural Information Processing Systems Datasets and Benchmarks Track (Round 1)*, 2021. URL <https://openreview.net/forum?id=r8IvOsnHchr>.
- Nikolay Laptev and Saeed Amizadeh. Yahoo! webscope dataset ydata-labeled-time-series-anomalies-v1.0. *CoRR*, 2020. URL <https://webscope.sandbox.yahoo.com/catalog.php?datatype=s&did=70>.
- Alexander Lavin and Subutai Ahmad. Evaluating real-time anomaly detection algorithms - the numenta anomaly benchmark. *CoRR*, abs/1510.03336, 2015. URL <http://arxiv.org/abs/1510.03336>.
- Kwonjoon Lee, Subhransu Maji, Avinash Ravichandran, and Stefano Soatto. Meta-learning with differentiable convex optimization. In *Proceedings of the IEEE/CVF Conference on Computer Vision and Pattern Recognition*, pp. 10657–10665, 2019.

- Fei Tony Liu, Kai Ming Ting, and Zhi-Hua Zhou. Isolation forest. In Fosca Giannotti, Dimitrios Gunopulos, Franco Turini, Carlo Zaniolo, Naren Ramakrishnan, and Xindong Wu (eds.), *Proceedings of the Eighth IEEE International Conference on Data Mining*, pp. 413 – 422, United States of America, 2008. IEEE, Institute of Electrical and Electronics Engineers. ISBN 9780769535029. URL <https://ieeexplore.ieee.org/xpl/conhome/4781077/proceeding>. IEEE International Conference on Data Mining 2008, ICDM 2008 ; Conference date: 15-12-2008 Through 19-12-2008.
- Song Liu, Makoto Yamada, Nigel Collier, and Masashi Sugiyama. Change-point detection in time-series data by relative density-ratio estimation. In *Structural, Syntactic, and Statistical Pattern Recognition*, pp. 363–372, Berlin, Heidelberg, 2012. Springer Berlin Heidelberg. ISBN 978-3-642-34166-3.
- Mohsin Munir, Shoaib Ahmed Siddiqui, Andreas Dengel, and Sheraz Ahmed. Deepant: A deep learning approach for unsupervised anomaly detection in time series. *IEEE Access*, 7:1991–2005, 2019. doi: 10.1109/ACCESS.2018.2886457.
- XuanLong Nguyen, Martin J. Wainwright, and Michael I. Jordan. Estimating divergence functionals and the likelihood ratio by convex risk minimization. *IEEE Transactions on Information Theory*, 56(11):5847–5861, Nov 2010. ISSN 1557-9654. doi: 10.1109/tit.2010.2068870. URL <http://dx.doi.org/10.1109/TIT.2010.2068870>.
- Boris N. Oreshkin, Dmitri Carпов, Nicolas Chapados, and Yoshua Bengio. N-BEATS: neural basis expansion analysis for interpretable time series forecasting. *CoRR*, abs/1905.10437, 2019. URL <http://arxiv.org/abs/1905.10437>.
- Ewan S Page. Continuous inspection schemes. *Biometrika*, 41(1/2):100–115, 1954.
- CE. Rasmussen and CKI. Williams. *Gaussian Processes for Machine Learning*. Adaptive Computation and Machine Learning. MIT Press, Cambridge, MA, USA, January 2006.
- Morten Ravn and Harald Uhlig. On adjusting the hodrick-prescott filter for the frequency of observations. *The Review of Economics and Statistics*, 84:371–375, 02 2002. doi: 10.1162/003465302317411604.
- Shebuti Rayana and Leman Akoglu. Less is more: Building selective anomaly ensembles with application to event detection in temporal graphs. In Suresh Venkatasubramanian and Jieping Ye (eds.), *Proceedings of the 2015 SIAM International Conference on Data Mining, Vancouver, BC, Canada, April 30 - May 2, 2015*, pp. 622–630. SIAM, 2015. doi: 10.1137/1.9781611974010.70. URL <https://doi.org/10.1137/1.9781611974010.70>.
- Evan Sandhaus. The new york times annotated corpus ldc2008t19. web download. *Linguistic Data Consortium, Philadelphia*, 6(12):e26752, 2008.
- Bernhard Schölkopf, Robert C Williamson, Alex Smola, John Shawe-Taylor, and John Platt. Support vector method for novelty detection. In S. Solla, T. Leen, and K. Müller (eds.), *Advances in Neural Information Processing Systems*, volume 12. MIT Press, 2000. URL <https://proceedings.neurips.cc/paper/1999/file/8725fb777f25776ffa9076e44fcfd776-Paper.pdf>.
- Rajat Sen, Hsiang-Fu Yu, and Inderjit S Dhillon. Think globally, act locally: A deep neural network approach to high-dimensional time series forecasting. In H. Wallach, H. Larochelle, A. Beygelzimer, F. d’Alché-Buc, E. Fox, and R. Garnett (eds.), *Advances in Neural Information Processing Systems*, volume 32. Curran Associates, Inc., 2019. URL <https://proceedings.neurips.cc/paper/2019/file/3a0844cee4fcf57de0c71e9ad3035478-Paper.pdf>.
- Lifeng Shen, Zhuocong Li, and James Kwok. Timeseries anomaly detection using temporal hierarchical one-class network. In H. Larochelle, M. Ranzato, R. Hadsell, M. F. Balcan, and H. Lin (eds.), *Advances in Neural Information Processing Systems*, volume 33, pp. 13016–13026. Curran Associates, Inc., 2020. URL <https://proceedings.neurips.cc/paper/2020/file/97e401a02082021fd24957f852e0e475-Paper.pdf>.

- Ya Su, Youjian Zhao, Chenhao Niu, Rong Liu, Wei Sun, and Dan Pei. Robust anomaly detection for multivariate time series through stochastic recurrent neural network. In *Proceedings of the 25th ACM SIGKDD International Conference on Knowledge Discovery & Data Mining, KDD '19*, pp. 2828–2837, New York, NY, USA, 2019. Association for Computing Machinery. ISBN 9781450362016. doi: 10.1145/3292500.3330672. URL <https://doi.org/10.1145/3292500.3330672>.
- Peter Tiño. Dynamical systems as temporal feature spaces. *CoRR*, abs/1907.06382, 2019. URL <http://arxiv.org/abs/1907.06382>.
- Michael E Tipping. Sparse bayesian learning and the relevance vector machine. *Journal of machine learning research*, 1(Jun):211–244, 2001.
- Michael Tsang, Hanpeng Liu, Sanjay Purushotham, Pavankumar Murali, and Yan Liu. Neural interaction transparency (nit): Disentangling learned interactions for improved interpretability. In S. Bengio, H. Wallach, H. Larochelle, K. Grauman, N. Cesa-Bianchi, and R. Garnett (eds.), *Advances in Neural Information Processing Systems*, volume 31. Curran Associates, Inc., 2018. URL <https://proceedings.neurips.cc/paper/2018/file/74378afe5e8b20910cf1f939e57f0480-Paper.pdf>.
- Vladimir N. Vapnik. *Statistical Learning Theory*. Wiley-Interscience, 1998.
- Thomas Wolf, Lysandre Debut, Victor Sanh, Julien Chaumond, Clement Delangue, Anthony Moi, Pierric Cistac, Tim Rault, Rémi Louf, Morgan Funtowicz, Joe Davison, Sam Shleifer, Patrick von Platen, Clara Ma, Yacine Jernite, Julien Plu, Canwen Xu, Teven Le Scao, Sylvain Gugger, Mariama Drame, Quentin Lhoest, and Alexander M. Rush. Transformers: State-of-the-art natural language processing. In *Proceedings of the 2020 Conference on Empirical Methods in Natural Language Processing: System Demonstrations*, pp. 38–45, Online, October 2020. Association for Computational Linguistics. URL <https://www.aclweb.org/anthology/2020.emnlp-demos.6>.
- Jiehui Xu, Haixu Wu, Jianmin Wang, and Mingsheng Long. Anomaly transformer: Time series anomaly detection with association discrepancy. *arXiv preprint arXiv:2110.02642*, 2021.
- Emmanuel Yashchin. Performance of cusum control schemes for serially correlated observations. *Technometrics*, 35(1):37–52, 1993. ISSN 00401706. URL <http://www.jstor.org/stable/1269288>.
- Chin-Chia Michael Yeh, Yan Zhu, Liudmila Ulanova, Nurjahan Begum, Yifei Ding, Hoang Anh Dau, Diego Furtado Silva, Abdullah Mueen, and Eamonn Keogh. Matrix profile i: All pairs similarity joins for time series: A unifying view that includes motifs, discords and shapelets. In *2016 IEEE 16th International Conference on Data Mining (ICDM)*, pp. 1317–1322, 2016. doi: 10.1109/ICDM.2016.0179.
- Luca Zancato and Alessandro Chiuso. A novel deep neural network architecture for non-linear system identification. *IFAC-PapersOnLine*, 54(7):186–191, 2021. ISSN 2405-8963. doi: <https://doi.org/10.1016/j.ifacol.2021.08.356>. URL <https://www.sciencedirect.com/science/article/pii/S2405896321011307>. 19th IFAC Symposium on System Identification SYSID 2021.
- Seyedjamal Zolhavarieh, Saeed Aghabozorgi, and Ying Wah Teh. A Review of Subsequence Time Series Clustering. *TheScientificWorldJournal*, 2014:312521, 2014. ISSN 1537-744X. doi: 10.1155/2014/312521. URL <http://www.pubmedcentral.nih.gov/articlerender.fcgi?artid=4130317&tool=pmcentrez&rendertype=abstract>.
- Bo Zong, Qi Song, Martin Renqiang Min, Wei Cheng, Cristian Lumezanu, Daeki Cho, and Haifeng Chen. Deep autoencoding gaussian mixture model for unsupervised anomaly detection. In *International Conference on Learning Representations*, 2018. URL <https://openreview.net/forum?id=BJJLHbb0->.

A APPENDIX

A.1 IMPLEMENTATION

Given two scalar time series x and φ , we denote their time convolution g as: $g(t) := (\varphi * x)(t) := \sum_{i=-\infty}^{\infty} \varphi(i)x(t-i)$. We say that g is the causal convolution of x and φ if $\varphi(t) = 0$ for $t < 0$, so that the output $g(t)$ does not depend on future values of x (w.r.t. current time index t). In the following, we shall give a particular interpretation to the signals x and φ : x will be the input signal to a filter parametrized by an impulse response φ (kernel of the filter). Note any (causal) convolution is defined by an infinite summation for each given time t . Therefore it is customary, when implementing convolutional filters, to consider a truncated sum of finite length. In practice, this is obtained assuming the filter impulse response is non-zero only in a finite window. The truncation is indeed an approximation of the complete convolution, nonetheless it is possible to prove that the approximation errors incurred due to truncation are guaranteed to be bounded under simple assumptions. To summarize, in the following we shall write $g(t) := (\varphi * x)(t)$ and mean that the impulse response of the causal filter φ is truncated on a window of a given length.

A.1.1 ARCHITECTURE

Let $Y_{t-n_p+1}^t \in \mathbb{R}^{n \times n_p}$ be the input data to our architecture at time step t (a window of n_p past time instants). The main blocks of the architecture are defined to encode trend, seasonality, stationary linear and non-linear part. In the following we shall denote each quantity related to a specific layer using either the subscripts {TREND, SEAS, LIN, TCN} or {0, 1, 2, 3}.

We shall denote the input of each block as $X_k \in \mathbb{R}^{n \times n_p}$ and the output as $\hat{X}_k \in \mathbb{R}^{n \times n_p}$ for $k = 0, 1, 2, 3$. The residual architecture we propose is defined by the following: $X_0 = Y_{t-n_p+1}^t$ and $X_k = X_{k-1} - \hat{X}_{k-1}$ for $k = 1, 2, 3$. At each layer we extract l_k temporal features from the input X_k . We denote the temporal features extracted from the input of the k -th block as: $G_k := G_k(X_k) \in \mathbb{R}^{l_k \times n_p}$. The i -th column of the feature matrix G_k is a feature vector (of size l_k) extracted from the input X_k up to time $t - n_p - i$. To do so, we use causal convolutions of the input signal X_k with a set of filter banks (Bai et al., 2018).

A.1.2 INTERPRETABLE RESIDUAL TCN ON SCALAR TIME SERIES

Modeling Interpretable blocks: In this section, we shall describe the main design criteria of the linear module. For each interpretable layer (TREND, SEAS, LIN), we convolve the input signal with a filter bank designed to extract specific components of the input.

For example, consider the trend layer, denoting its scalar input time series by x and its output by g_{TREND} . Then g_{TREND} is defined as a multidimensional time series (of dimension $l_{\text{TREND}} := l_0$) obtained by stacking l_0 time series given by the convolution of x with l_0 causal linear filters: $\varphi_{\text{TREND}_i} * x$ for $i = 0, \dots, l_0 - 1$. In other words, $g_{\text{TREND}} := [\varphi_{\text{TREND}_1} * x, \varphi_{\text{TREND}_2} * x, \dots, \varphi_{\text{TREND}_{l_1}} * x]^T$. We denote the set of linear filters φ_{TREND_i} for $i = 0, \dots, l_0 - 1$ as $\mathcal{K}_{\text{TREND}}$ and parametrize each filter in $\mathcal{K}_{\text{TREND}}$ with its truncated impulse response (i.e. kernel) of length $k_0 := k_{\text{TREND}}$.

We interpret each time series in g_{TREND} as an approximation of the trend component of x computed with the i -th filter. We design each φ_{TREND_i} so that each filter extracts the trend of the input signal on different time scales (Ravn & Uhlig, 2002) (i.e., each filter outputs a signal with a different smoothness degree). We estimate the trend of the input signal by recombining the extracted trend components in g_{TREND} with the linear map a_{TREND} . Moreover, we predict the future trend of the input signal (on the next time-stamp) with the linear map b_{TREND} .

We construct the blocks that extract seasonality and linear part in a similar way.

Implementing Interpretable blocks: The input of each layer is given by a window of measurements of length n_p . We zero-pad the input signal so that the convolution of the input signal with the i -th filter is a signal of length n_p (note this introduces a spurious transient whose length is the length of the filter kernel). We therefore have the following temporal feature matrices: $G_0 = G_{\text{TREND}} \in \mathbb{R}^{l_0 \times n_p}$, $G_1 = G_{\text{SEAS}} \in \mathbb{R}^{l_1 \times n_p}$ and $G_2 = G_{\text{LIN}} \in \mathbb{R}^{l_2 \times n_p}$.

The output of each layer \hat{X}_k is an estimate of the trend, seasonal or stationary linear component of the input signal on the past interval of length n_p , so that we have $\hat{X}_k \in \mathbb{R}^{1 \times n_p}$ (same dimension as the input X_k). On the other hand, the linear predictor \hat{y}_k computed at each layer is a scalar. Intuitively, \hat{X}_k and \hat{y}_k should be considered as the best linear approximation of the trend, seasonality or linear part given block’s filter bank in the past and future. Our architecture performs the following computations: $\hat{X}_k := a_k^T G_k$ and $\hat{y}_k := \hat{X}_k b_k$ for $k = 0, 1, 2$ where $a_k \in \mathbb{R}^{l_k}$ and $b_k \in \mathbb{R}^{n_p}$. Note a_k combines features (uniformly in time) so that we can interpret it as a feature selector while b_k aggregates relevant features across different time indices to build the one-step ahead predictor. Depending on the time scale of the signals it is possible to choose b_k depending on the time index (similarly to the fading memory regularization). We experimented both the choice to make b_k canonical “vectors” and dense vectors. We found that choosing b_k as canonical vectors, whose non-zero entry is associated to the closest to the present time instat provides good empirical results on most cases.

Non-linear module The non-linear module is based on a standard TCN network. Its input is defined as $X_3 = Y_{t-n_p+1}^t - \hat{X}_0 - \hat{X}_1 - \hat{X}_2$, which is to be considered as a signal whose linearly predictable component has been removed. The TCN extracts a set of l_3 non-linear features $G_3(X_3) \in \mathbb{R}^{l_3 \times n_p}$ which we combine with linear maps as done for the previous layers. The j -th column of the non-linear features G_3 is computed using data up to time $t - n_p + j$ (due to the internal structure of a TCN network (Bai et al., 2018)). The linear predictor on top of G_3 is $\hat{y}_{\text{TCN}} := a_3^T G_3 b_3$, where $a_3 \in \mathbb{R}^{l_3}$ and $b_3 \in \mathbb{R}^{n_p}$.

Finally, the output of our time model is given by:

$$\hat{y}(t+1) = \sum_{k=0}^3 \hat{y}_k = \sum_{k=0}^3 \hat{X}_k b_k = \sum_{k=0}^3 a_k^T G_k(X_k) b_k.$$

A.1.3 INTERPRETABLE RESIDUAL TCN ON MULTI-DIMENSIONAL TIME SERIES

We extend our architecture to multi-dimensional time series according to the following principles: preserve interpretability (first module) and exploit global information to make local predictions (second module).

In this section, the input data to our model is $Y_{t-n_p+1}^t \in \mathbb{R}^{n \times n_p}$ (a window of length n_p from an n -dimensional time series).

Interpretable module: Each time series undergoes the sequence of 3 interpretable blocks independently from other time series: the filter banks are applied to each time series independently. Therefore, each time series is processed by the same filter banks: $\mathcal{K}_{\text{TREND}}$, $\mathcal{K}_{\text{SEAS}}$ and \mathcal{K}_{LIN} . For ease of notation we shall now focus only on the trend layer. Any other layer is obtained by substituting ‘TREND’ with the proper subscript (‘SEAS’ or ‘LIN’).

We denote by $G_{\text{TREND}}, i \in \mathbb{R}^{l_0 \times n_p}$ the set of time features extracted by the trend filter bank $\mathcal{K}_{\text{TREND}}$ from the i -th time series. Each feature matrix is then combined as done in the scalar setting using linear maps, which we now index by the time series index i : a_{TREND_i} and b_{TREND_i} . The rationale behind this choice is that each time series can exploit differently the extracted features. For instance, slow time series might need a different filter than faster ones (chosen using a_{TREND_i}) or might need to look at values further in the past (retrieved using b_{TREND_i}). We stack the combination vectors a_{TREND_i} and b_{TREND_i} into the following matrices: $\mathcal{A}_{\text{TREND}} = [a_{\text{TREND}_1}, a_{\text{TREND}_2}, \dots, a_{\text{TREND}_n}]^T \in \mathbb{R}^{n \times l_0}$ and $\mathcal{B}_{\text{TREND}} = [b_{\text{TREND}_1}, b_{\text{TREND}_2}, \dots, b_{\text{TREND}_n}]^T \in \mathbb{R}^{n \times n_p}$.

Non-linear module: The second (*non-linear*) module aggregates global statistics from different time series (Sen et al., 2019) using a TCN model. It takes as input the prediction residual of the linear module and outputs a matrix $G_{\text{TREND}}(Y_{t-n_p+1}^t) \in \mathbb{R}^{l_3 \times n_p}$ where l_3 is the number of output features that are extracted by the TCN model (which is a design parameter). The j -th column of the non-linear features $G_{\text{TREND}}(Y_{t-n_p+1}^t)$ is computed using data up to time $t - p + j$, where p is the “receptive” field of the TCN ($p < n_p$). This is due to the internal structure of a TCN network (Bai et al., 2018) which relies on causal convolutions and typically scales as $O(2^h)$ where h is the number of TCN hidden layers (the deeper the TCN the longer its receptive field). As done for the time features extracted by the interpretable blocks, we build a linear predictor on top of $G_{\text{TREND}}(Y_{t-n_p+1}^t)$ for each single time series independently: the predictor for the i -th time series is given by: $\hat{y}_{\text{TCN}}(t +$

$1)_i := a_i^T G_{\text{TREND}}(Y_{t-n_p+1}^t) b_i$ where $a_i \in \mathbb{R}^{l_3}$ and $b_i \in \mathbb{R}^{n_p}$. We stack the combination vectors $a_{\text{TCN}i}$ and $b_{\text{TCN}i}$ into the following matrices: $\mathcal{A}_{\text{TCN}} = [a_{\text{TCN}1}, a_{\text{TCN}2}, \dots, a_{\text{TCN}n}]^T \in \mathbb{R}^{n \times l_3}$ and $\mathcal{B}_{\text{TCN}} = [b_{\text{TCN}1}, b_{\text{TCN}2}, \dots, b_{\text{TCN}n}]^T \in \mathbb{R}^{n \times n_p}$.

Finally, the outputs of the predictor on the i -th time series are given by:

$$\hat{y}(t+1)_i = \sum_{k \in \{\text{TREND}, \text{SEAS}, \text{LIN}\}} a_{k_i}^T G_{k_i} b_{k_i} + a_{\text{TCN}i}^T G_{\text{TCN}} b_{\text{TCN}i} \quad (5)$$

A.1.4 BLOCK STRUCTURE AND INITIALIZATION

In this section, we shall describe the internal structure and the initialization of each block.

Structure: Each filter is implemented by means of depth-wise causal 1-D convolutions (Bai et al., 2018). We call the tensor containing the k -th block’s kernel parameters $\mathcal{K}_k \in \mathbb{R}^{l_k \times N_k}$, where l_k and N_k are the block’s number of filters and block’s kernel size, respectively (without loss of generality, we assume all filters have the same dimension). Each filter (causal 1D-convolution) is parametrized by the values of its impulse response parameters (kernel parameters). When we learn a filter bank, we mean that we optimize over the kernel values for each filter jointly. For multidimensional time series, we apply the filter banks to each time series independently (depth-wise convolution) and improve filter learning by sharing kernel parameters across different time series.

Initialization: The *first block* (trend) is initialized using l_0 causal Hodrick Prescott (HP) filters (Ravn & Uhlig, 2002) of kernel size N_0 . HP filters are widely used to extract trend components of signals (Ravn & Uhlig, 2002). In general a HP filter is used to obtain from a time series a smoothed curve which is not sensitive to short-term fluctuations and more sensitive to long-term ones (Ravn & Uhlig, 2002). In general, a HP filter is parametrized by a hyper-parameter λ_{HP} which defines the regularity of the filtered signal (the higher λ_{HP} , the smoother the output signal). We initialize each filter with λ_{HP} chosen uniformly in log-scale between 10^3 and 10^9 . Note the impulse response of these filters decays to zero (i.e., the latest samples from the input time series are the most influential ones). When we learn the optimal set of trend filter banks, we do not consider them parametrized by λ_{HP} and search for the optimal λ_{HP} . Instead, we optimize over the impulse response parameters of the kernel which we do not assume live in any manifold (e.g., the manifold of HP filters). Since this might lead to optimal filters which are not in the class of HP filters, we impose a regularization which penalizes the distance of the optimal impulse response parameters from their initialization.

The *second block* (seasonal part) is initialized using l_1 periodic kernels which are obtained as linear filters whose poles (i.e., frequencies) are randomly chosen on the unit circle (this guarantees to span a range of different frequencies). Note the impulse responses of these filters do not go to zero (their memory does not fade away). Similarly to the HP filter bank, we do not optimize the filters over frequencies, but rather we optimize them over their impulse response (kernel parameters). This optimization does not preserve the strict periodicity of filters. Therefore, in order to keep the optimal impulse response close to initialization values (purely periodic), we exploit weight regularization by penalizing the distance of the optimal set of kernel values from initialization values.

The *third block* (stationary linear part) is initialized using l_2 randomly chosen linear filters whose poles lie inside the unit circle, as done in (Farahmand et al., 2017). As the number of filters l_2 increases, this random filter bank is guaranteed to be a universal approximator of any (stationary) linear system (see (Farahmand et al., 2017) for details).

Remark: This block could approximate any trend and periodic component. However, we assume to have factored out both trend and periodicities in the previous blocks.

The last module (*non-linear part*) is composed by a randomly initialized TCN model. We employ a TCN model due to its flexibility and capability to model both long-term and short-term non-linear dependencies. As is standard practice, we exploit dilated convolutions to increase the receptive field and make the predictions of the TCN (on the future horizon) depend on the most relevant past (Bai et al., 2018).

Remark: Our architecture provides an interpretable justification of the initialization scheme proposed for TCN in (Sen et al., 2019). In particular our convolutional architecture allows us to handle

high-dimensional time series data without a-priori standardization (e.g., trend or seasonality removal).

A.2 AUTOMATIC COMPLEXITY DETERMINATION (FADING MEMORY REGULARIZATION)

In this section, we shall introduce a regularization scheme called *fading regularization*, to constrain TCN representational capabilities.

The output of the TCN model is $G(Y_{t-n_p+1}^t) \in \mathbb{R}^{l_3 \times n_p}$ where l_3 is the number of output features extracted by the TCN model. The predictor build from TCN features is given by: $a_{\text{TCN}_i}^T G_{\text{TCN}}(Y_{t-n_p+1}^t) b_{\text{TCN}_i}$, where the predictor $b_{\text{TCN}_i} \in \mathbb{R}^{n_p}$ takes as input a linear combination of the TCN features (weighted by a_{TCN_i}). The j -th column of the non-linear features $G(Y_{t-n_p+1}^t)$ is computed using data up to time $t - n_p + j$ (due to causal convolutions used in the internal structure of the TCN network (Bai et al., 2018)). One expects that the influence on the TCN predictor as j increases should increase too (in case $j = n_p$, the statistic is the one computed on the closest window of time w.r.t. present time stamp). Clearly, the exact *relevance* on the output is not known a priori and needs to be estimated. In other words, the predictor should be less sensitive to statistics (features) computed on a far past, a property which is commonly known as *fading memory*. Currently, this property is not built in the predictor b_{TCN_i} , which treats each time instant equally and might overfit while trying to explain the future by looking into far and possibly non-relevant past. In order to constrain model complexity and reduce overfitting, we impose the fading memory property on our predictor by employing a specific regularization which we now describe.

A.2.1 FADING MEMORY IN SCALAR TIME SERIES

We now follow the same notation and assumptions used in Section 4.1 which we now repeat for completeness.

We consider a scalar time series so that the TCN-based future predictor given the past n_p measures can be written as: $\hat{y}_{\text{TCN}}(t+1) = a^T G_{\text{TCN}}(Y_{t-n_p+1}^t) b = \hat{X}_k b$. We shall assume that innovations (optimal prediction errors) are Gaussian, so that $y(t+1) | Y_{t-n_p+1}^t \sim \mathcal{N}(F^*(Y_{t-n_p+1}^t), \eta^2)$, where F^* is the optimal predictor of the future values given the past. Note that this assumption does not restrict our framework and is used only to justify the use of the squared loss to learn the regression function of the predictor. In practice, we do not know the optimal F^* and we approximate it with our parametric model. For ease of exposition, we group all the architecture parameters except b in the weight vector W (linear filters parameters $\mathcal{K}_{\text{TREND}}, \mathcal{K}_{\text{SEAS}}, \mathcal{K}_{\text{LIN}}$, linear module recombination weights $\mathcal{A}_{\text{TREND}}, \mathcal{A}_{\text{SEAS}}, \mathcal{A}_{\text{LIN}}$, $\mathcal{B}_{\text{TREND}}, \mathcal{B}_{\text{SEAS}}, \mathcal{B}_{\text{LIN}}$, and TCN kernel parameters and recombination coefficients \mathcal{A}_{TCN} etc.). We write the conditional likelihood of the future given the past data of our parametric model as:

$$p(Y_{t+1}^{t+n_a} | b, W, Y_{t-n_p+1}^t) = \prod_{k=1}^{n_a} p(y(t+k) | b, W, Y_{t+k-n_p}^{t+k-1}) \quad (6)$$

To make the notation simpler, we shall denote by $Y_f := Y_{t+1}^{t+n_a} \in \mathbb{R}^{n_a}$ the set of future outputs over which the predictor is computed and we shall use $\hat{Y}_{b,W} \in \mathbb{R}^{n_a}$ as the predictor's outputs. Moreover, we shall drop the dependency on the conditioning past $Y_{t-n_p+1}^t$ (which is present in any conditional distribution). Equation (6) becomes: $p(Y_f | b, W) = \prod_{k=1}^{n_a} p(y(t+k) | b, W)$. The optimal set of parameters b^* and W^* in a Bayesian framework is computed by maximizing the posterior on the parameters given the data:

$$p(b, W | Y_f) \propto p(Y_f | b, W) p(b) p(W) \quad (7)$$

where $p(b)$ is the prior on the predictor and $p(W)$ is the prior on the remaining parameters. We encode in $p(b)$ our prior belief that the complexity of the predictor should not be too high and therefore it should only depend on the *most relevant past*.

Remark: The prior does not induce hard constraints. It rather biases the optimal predictor coefficients towards the prior belief. This is clear by looking at the negative log-posterior which can be directly interpreted as the loss function to be minimized: $-\log p(b, W | Y_f) = -\log p(Y_f | b, W) - \log p(b) - \log p(W)$. In particular, the first term $\log p(Y_f | b, W)$ is the data fitting term

(only influenced by the data). Both $\log p(b)$ and $\log p(W)$ do not depend on the available data and can be interpreted as regularization terms that bound the complexity of the predictor function.

The main idea is to reduce the sensitivity of the predictor on time instants that are far in the past. We therefore enforce the *fading memory* assumption on $p(b)$ by assuming that the components of $b \in \mathbb{R}^{n_p}$ have zero mean and exponentially decaying variances:

$$\mathbb{E}b_j = 0 \text{ and } \mathbb{E}b_{n_p-j-1}^2 = \kappa\lambda^j \text{ for } j = 0, \dots, n_p - 1 \quad (8)$$

where $\kappa \in \mathbb{R}^+$ and $\lambda \in (0, 1)$. Note the larger variance (larger scale) is associated to temporal indices close to the present time t .

Remark: To specify the prior, we need a density function $p(b)$ but up to now we only specified constraints on the first and second order moments. We therefore need to constrain the parametric family of prior distributions we consider. Any choice on the class of prior distributions lead to different optimal estimators. Among all the possible choices of prior families we choose the maximum entropy prior (Cover & Thomas, 1991). Under constraints on first and second moment, the maximum entropy family of priors is the exponential family (Cover & Thomas, 1991). In our setting, we can write it as:

$$\log p_{\lambda, \kappa}(b) \propto -\|b\|_{\Lambda^{-1}}^2 - \log |\Lambda| \quad (9)$$

where $\Lambda \in \mathbb{R}^{n_p \times n_p}$ is a diagonal matrix whose elements are $\Lambda_{j,j} = \kappa\lambda^j$ for $j = 0, \dots, n_p - 1$.

The parameter λ represents how fast the predictor's output 'forgets' the past: the smaller λ , the lower the complexity. In practice, we do not have access to this information and indeed we need to estimate λ from the data.

One would be tempted to estimate jointly W, b, λ, κ (and possibly η) by minimizing the negative log of the joint posterior:

$$\arg \min_{b, W, \lambda, \kappa} \frac{1}{\eta^2} \|Y_f - \hat{Y}_{b, W}\|^2 + \log(\eta^2) - \log(p_{\lambda, \kappa}(B)) - \log(p(W)) \quad (10)$$

Unfortunately, this leads to a degeneracy since the joint negative log posterior goes to $-\infty$ when $\lambda \rightarrow 0$.

Bayesian learning formulation for fading memory regularization: The parameters describing the prior (such as λ) are typically estimated by maximizing the marginal likelihood, i.e., the likelihood of the data once the parameters (b, W) have been integrated out. Unfortunately, the task of computing (or even approximating) the marginal likelihood in this setup is prohibitive and one would need to resort to Monte Carlo sampling techniques. While this is an avenue worth investigating, we preferred to adopt the following variational strategy inspired by the linear setup.

Indeed, the model structure we consider is linear in b and we can therefore stack the predictions of each available time index t to get the following linear predictor on the whole future data: $\hat{Y}_{b, W} = F_W b$ where $F_W \in \mathbb{R}^{n_a \times n_p}$ and its rows are given by $\hat{X}_{\text{TCN}}(Y_{i-n_p+1}^i)$ for $i = t, \dots, t + n_a - 1$.

We are now ready to find an upper bound to the marginal likelihood associated to the posterior given by Equation (7) with marginalization taken only w.r.t. b .

Proposition A.1 (from (Tipping, 2001)) *The optimal value of a regularized linear least squares problem with feature matrix F and parameters b is given by the following equation:*

$$\arg \min_b \frac{1}{\eta^2} \|Y_f - Fb\|^2 + b^\top \Lambda^{-1} b = Y_f^\top \Sigma^{-1} Y_f \quad (11)$$

with $\Sigma := F\Lambda F^\top + \eta^2 I$.

Equation (11) guarantees that

$$\frac{1}{\eta^2} \|Y_f - Fb\|^2 + b^\top \Lambda^{-1} b + \log |\Sigma| \geq Y_f^\top \Sigma^{-1} Y_f + \log |\Sigma|,$$

where the right hand side is (proportional to) the negative marginal likelihood with marginalization taken *only* w.r.t. b . Therefore, for fixed a W ,

$$\frac{1}{\eta^2} \left\| Y_f - \hat{Y}_{b,W} \right\|^2 + b^\top \Lambda^{-1} b + \log |F_W \Lambda F_W^\top + \eta^2 I|$$

is an upper bound of the marginal likelihood with marginalization over b and does not suffer of the degeneracy alluded at before.

With this considerations in mind, and inserting back the optimization over W , the overall optimization problem we solve is

$$\begin{aligned} \arg \min_{b,W,\lambda \in (0,1), \kappa > 0} & \frac{1}{\eta^2} \left\| Y_f - \hat{Y}_{b,W} \right\|^2 + \|b\|_{\Lambda^{-1}}^2 \\ & + \log |F_W \Lambda F_W + \eta^2 I| + \log p(W) \end{aligned} \quad (12)$$

Remark: $\log p(W)$ defines the regularization applied on the remaining parameters of our architecture. In particular, we induce sparsity by applying L^1 regularization on $\mathcal{A}_{\text{TREND}}$, $\mathcal{A}_{\text{SEAS}}$, \mathcal{A}_{LIN} and \mathcal{A}_{TCN} . Also, we constrain filters parameters to stay close to initialization by applying L^2 regularization on $\mathcal{K}_{\text{TREND}}$, $\mathcal{K}_{\text{SEAS}}$ and \mathcal{K}_{LIN} .

A.2.2 FADING MEMORY IN MULTIVARIATE TIME SERIES

In the case of multivariate time series, fading regularization can be applied either with a single fading coefficient λ for all the time series or with different fading coefficients for each time series. In all the experiments in this paper, we chose to keep one single λ for all the time series. In practice, this choice is sub-optimal and might lead to more overfitting than treating each time series separately: the ‘dominant’ (slower) time series will highly influence the optimal λ .

A.2.3 FEATURES NORMALIZATION

We avoid the non-identifiability of the product $F_W b$ by exploiting batch normalization: we impose that different features have comparable means and scales across time indices $i = 0, \dots, n_p - 1$. Non-identifiability occurs due to the product $F_W b$, if features have different scales across time indices (i.e., columns of the matrix F_W) the benefit of fading regularization might reduced since it can happen that features associated with small b_i have large scale so that the overall contribution of the past does not fade. Hence we use batch normalization to normalize time features. Then we use an affine transformation (with parameters to be optimized) to jointly re-scale all the output blocks before the linear combination with b .

A.3 ALTERNATIVE CUMSUM DERIVATION AND INTERPRETATION

In this section, we describe an equivalent formulation of the CUMSUM algorithm we derived in the main paper. Before a change point, by construction we are under the distribution of the past. Therefore, $\log \frac{p_a(y)}{p_n(y)} \leq 0 \forall y$, which in turn means that the cumulative sum S_1^t will decrease as t increases (negative drift). After the change, the situation is opposite and the cumulative sum starts to show a positive drift, since we are sampling $y(i)$ from the future distribution p_a . This intuitive behaviour shows that the relevant information to detect a change point can be obtained directly from the cumulative sum (along timestamps). In particular, all we need to know is the difference between the value of the cumulative sum of log-likelihood ratios and its minimum value.

The CUMSUM algorithm can be expressed using the following equations: $v_t := S_1^t - m_t$, where $m_t := \min_{j, 1 \leq j \leq t} S_j^t$. The stopping time is defined as: $t_{\text{stop}} = \min\{t : v_t \geq \epsilon\} = \min\{t : S_1^t \geq m_t + \epsilon\}$. With the last equation, it becomes clear that the CUMSUM detection equation is simply a comparison of the cumulative sum of the log likelihood ratios along time with an adaptive threshold $m_t + \epsilon$. Note that the adaptive threshold keeps complete memory of the past ratios. The two formulations are equivalent because $S_1^t - m_t = h_t$.

A.4 VARIATIONAL APPROXIMATION OF THE LIKELIHOOD RATIO

In this section, we present some well known facts on f -divergences and their variational characterization. Most of the material and the notation is from (Nguyen et al., 2010). Given a probability distribution \mathbb{P} and a random variable f measurable w.r.t. \mathbb{P} , we use $\int f d\mathbb{P}$ to denote the expectation of f under \mathbb{P} . Given samples $x(1), \dots, x(n)$ from \mathbb{P} , the empirical distribution \mathbb{P}_n is given by $\mathbb{P}_n = \frac{1}{n} \sum_{i=1}^n \delta_{x(i)}$. We use $\int f d\mathbb{P}_n$ as a convenient shorthand for the empirical expectation $\frac{1}{n} \sum_{i=1}^n f(x(i))$.

Consider two probability distributions \mathbb{P} and \mathbb{Q} , with \mathbb{P} absolutely continuous w.r.t. \mathbb{Q} . Assume moreover that both distributions are absolutely continuous with respect to the Lebesgue measure μ , with densities p_0 and q_0 , respectively, on some compact domain $\mathcal{X} \subset \mathbb{R}^d$.

Variational approximation of the f -divergence: The f -divergence between \mathbb{P} and \mathbb{Q} is defined as (Nguyen et al., 2010)

$$D_f(\mathbb{P}, \mathbb{Q}) := \int p_0 f\left(\frac{q_0}{p_0}\right) d\mu \quad (13)$$

where $f : \mathbb{R} \rightarrow \mathbb{R}$ is a convex and lower semi-continuous function. Different choices of f result in a variety of divergences that play important roles in various fields (Nguyen et al., 2010). Equation (13) is usually replaced by the variational lower bound:

$$D_f(\mathbb{P}, \mathbb{Q}) \geq \sup_{\phi \in \Phi} \int [\phi d\mathbb{Q} - f^*(\phi) d\mathbb{P}] \quad (14)$$

and equality holds iff the subdifferential $\partial f\left(\frac{q_0}{p_0}\right)$ contains an element of Φ . Here f^* is defined as the convex dual function of f .

In the following, we are interested in divergences whose conjugate dual function is smooth (which in turn defines commonly used divergence measures such as KL and Pearson divergence), so that we shall assume that f is convex and differentiable. Under this assumption, the notion of subdifferential is not required and the previous statement reads as: *equality holds iff $\partial f\left(\frac{q_0}{p_0}\right) = \phi$ for some $\phi \in \Phi$.*

Remark: The infinite-dimensional optimization problem in Equation (14) can be written as $D_f(\mathbb{P}, \mathbb{Q}) = \sup_{\phi \in \Phi} \mathbb{E}_{\mathbb{Q}} \phi - \mathbb{E}_{\mathbb{P}} f^*(\phi)$.

In practice, one can have an estimator of any f -divergence restricted to a functional class Φ by solving Equation (14) (Nguyen et al., 2010). Moreover, when \mathbb{P} and \mathbb{Q} are not known one can approximate them using their empirical counterparts: \mathbb{P}_n and \mathbb{Q}_n . Then an empirical estimate of the f -divergence is: $\hat{D}_f(\mathbb{P}, \mathbb{Q}) = \sup_{\phi \in \Phi} \mathbb{E}_{\mathbb{Q}_n} \phi - \mathbb{E}_{\mathbb{P}_n} f^*(\phi)$.

Approximation of the likelihood ratio: An estimate of the likelihood ratio can be directly obtained from the variational approximation of f -divergences. The key observation is the following: *equality on Equation (14) is achieved iff $\phi = \partial f\left(\frac{q_0}{p_0}\right)$.* This tells us that the optimal solution to the variational approximation provides us with an estimator of the composite function $\partial f\left(\frac{q_0}{p_0}\right)$ of the likelihood ratio $\frac{q_0}{p_0}$. As long as we can invert ∂f , we can uniquely determine the likelihood ratio.

In the following, we shall get an empirical estimator of the likelihood ratio in two separate steps. We first solve the following:

$$\hat{\phi}_n := \arg \max_{\phi \in \Phi} \mathbb{E}_{\mathbb{Q}_n} \phi - \mathbb{E}_{\mathbb{P}_n} f^*(\phi) \quad (15)$$

which returns an estimator of $\partial f\left(\frac{q_0}{p_0}\right)$, not the ratio itself. And then we apply the inverse of ∂f to $\hat{\phi}_n$. We therefore have a family of estimation methods for the likelihood function by simply ranging over choices of f .

Remark: If f is not differentiable, then we cannot invert ∂f but we can obtain estimators of other functions of the likelihood ratio. For instance, we can obtain an estimate of the thresholded likelihood ratio by using a convex function whose subgradient is the sign function centered at 1.

A.4.1 LIKELIHOOD RATIO ESTIMATION WITH PEARSON DIVERGENCE

In this section, we show how to estimate the likelihood ratio when the Pearson divergence is used. With this choice, many computations simplify and we can write the estimator of the likelihood ratio

in closed form. Other choices (such as the Kullback-Leibler divergence) are possible and legitimate, but usually do not lead to closed form expressions (see (Nguyen et al., 2010)).

The Pearson, or χ^2 , divergence is defined by the following choice: $f(t) := \frac{(t-1)^2}{2}$. The associated convex dual function is :

$$f^*(v) = \sup_{u \in \mathbb{R}} \left\{ uv - \frac{(u-1)^2}{2} \right\} = \frac{v^2}{2} + v.$$

Therefore the Pearson divergence is characterized by the following:

$$PE(\mathbb{P}||\mathbb{Q}) := \int p_0 \left(\frac{q_0}{p_0} - 1 \right)^2 d\mu \geq \sup_{\phi \in \Phi} \mathbb{E}_{\mathbb{Q}} \phi - \frac{1}{2} \mathbb{E}_{\mathbb{P}} \phi^2 - \mathbb{E}_{\mathbb{P}} \phi. \quad (16)$$

Solving the lower bound for the optimal ϕ provides us an estimator of $\partial f\left(\frac{q_0}{p_0}\right) = \frac{q_0}{p_0} - 1$. For the special case of the Pearson divergence, we can apply a change of variables which preserves convexity of the variational optimization problem Equation (16) and provides a more straightforward interpretation. Let the new variable be $z := \phi + 1$ with $z \in \mathcal{Z}$, which in this case is nothing but the inverse function of ∂f . We get

$$\sup_{\phi \in \Phi} \mathbb{E}_{\mathbb{Q}} \phi - \frac{1}{2} \mathbb{E}_{\mathbb{P}} \phi^2 - \mathbb{E}_{\mathbb{P}} \phi = \sup_{z \in \mathcal{Z}} \mathbb{E}_{\mathbb{Q}} z - \frac{1}{2} \mathbb{E}_{\mathbb{P}} z^2 - \frac{1}{2} \quad (17)$$

It is now trivial to see that z is a ‘direct’ approximator of the likelihood ratio (i.e., it does not estimate a composite map of the likelihood ratio). Therefore for simplicity, we shall employ

$$\arg \min_{\phi \in \Phi} \frac{1}{2} \mathbb{E}_{\mathbb{P}} \phi^2 - \mathbb{E}_{\mathbb{Q}} \phi \quad (18)$$

to build our ‘direct’ estimator of the likelihood ratio.

Let the samples from \mathbb{P} and \mathbb{Q} be, respectively, $x_p(i)$ with $i = 1, \dots, n_p$ and $x_q(i)$ with $i = 1, \dots, n_q$. We define the empirical estimator of the likelihood ratio $\hat{\phi}_n$:

$$\hat{\phi}_n = \arg \min_{\phi \in \Phi} \frac{1}{2n_p} \sum_{i=1}^{n_p} \phi(x_p(i))^2 - \frac{1}{n_q} \sum_{i=1}^{n_q} \phi(x_q(i)). \quad (19)$$

A closed form solution: Up to now we have not defined in which class of functions our approximator ϕ lives. As done in (Nguyen et al., 2010; Liu et al., 2012), we choose $\phi \in \Phi$ where Φ is a RKHS induced by the kernel k .

We exploit the representer theorem to write a general function within Φ as:

$$\phi(x) = \sum_{i=1}^{n_{tr}} k(x, x_{tr}(i)) \alpha_i,$$

where we use n_{tr} data which are the centers of the kernel sections used to approximate the unknown likelihood ratio (how to choose these centers is important and determines the approximation properties of $\hat{\phi}_n$). For now, we do not specify which data should be used as centers (we can use either data from \mathbb{P}_n or from \mathbb{Q}_n or from both or simply use user specified locations).

Let us define the following kernel matrices: $K_p := K(X_p, X_{tr}) \in \mathbb{R}^{n_p \times n_{tr}}$, $K_q := K(X_q, X_{tr}) \in \mathbb{R}^{n_q \times n_{tr}}$, where $X_p := \{x_p(i)\}$, $X_q := \{x_q(i)\}$ and $X_{tr} := \{x_{tr}(i)\}$.

We therefore have:

$$\begin{aligned}
\hat{\phi}_n &= \arg \min_{\phi \in \Phi} \frac{1}{2n_p} \sum_{i=1}^{n_p} \phi(x_p(i))^2 - \frac{1}{n_q} \sum_{i=1}^{n_q} \phi(x_q(i)) \\
&= \arg \min_{\alpha, \alpha \geq 0} \frac{1}{2n_p} \sum_{i=1}^{n_p} \left(\sum_{j=1}^{n_{tr}} k(x_p(i), x_{tr}(j)) \alpha_j \right)^2 \\
&\quad - \frac{1}{n_a} \sum_{i=1}^{n_a} \sum_{j=1}^{n_{tr}} k(x_q(i), x_{tr}(j)) \alpha_j \\
&= \arg \min_{\alpha, \alpha \geq 0} \frac{1}{2n_p} \alpha^T K_p^T K_p \alpha - \frac{1}{n_a} \mathbb{1}^T K_q \alpha
\end{aligned}$$

Remark: We impose the recombination coefficients α to be non negative since the likelihood ratio is a non negative quantity. The resulting optimization problem is a standard convex optimization problem with linear constraints which can be efficiently solved with Newton methods, nonetheless in general it does not admit any closed form solution.

We now relax the positivity constraints so that the optimal solution can be obtained in closed form. Moreover we add a quadratic regularization term as done in (Nguyen et al., 2010) which lead us to the following regularized optimization problem:

$$\arg \min_{\alpha} \frac{1}{2n_p} \alpha^T K_p^T K_p \alpha - \frac{1}{n_a} \mathbb{1}^T K_q \alpha + \frac{\gamma}{2} \|\alpha\|_{\Phi}^2$$

whose solution is trivially given by:

$$\hat{\alpha} = \frac{n_p}{n_a} \left(K_p^T K_p + n_p \gamma I_{n_{tr}} \right)^{-1} K_q^T \mathbb{1} := \frac{n_p}{n_a} H^{-1} K_q^T \mathbb{1} \quad (20)$$

The estimator of the likelihood ratio for an arbitrary location x is given by the following:

$$\begin{aligned}
\frac{p_q(x)}{p_p(x)} &\approx \hat{\phi}_n(x) = K(x, X_{tr}) \hat{\alpha} \\
&= \frac{n_p}{n_a} K(x, X_{tr}) \left(K_p^T K_p + n_p \gamma I_{n_{tr}} \right)^{-1} K_q^T \mathbb{1} \quad (21)
\end{aligned}$$

Remark: In the following we shall exploit RBF kernels which are defined by the length scales σ .

A.5 SUBSPACE LIKELIHOOD RATIO ESTIMATION AND CUMSUM

In this section we describe our subspace likelihood ratio estimator and its relation to the CUMSUM algorithm. The CUMSUM algorithm requires to compute the likelihood ratio $\frac{p_a(y(t)|Y_c^{t-1})}{p_n(y(t)|Y_c^{t-1})}$ for each time t . We denote p_n as the normal density and p_a as the abnormal one (after the anomaly has occurred).

We shall proceed to express the conditional probability $p(y(t) | Y_1^{t-1})$ using our predictor. In particular it is always possible to express the optimal (unknown) one-step ahead predictor as:

$$\hat{y}_{t|t-1} = F^*(Y_{t-K+1}^t) := \mathbb{E}[y(t) | Y_{t-K+1}^t] \quad (22)$$

which is a deterministic function given the past of the time series (whose length is K). So that the data density distribution can be written in innovation form (based on the optimal prediction error) as:

$$y(t) = F^*(Y_{t-K+1}^t) + e(t) \quad (23)$$

where $e(t) := y(t) - F^*(Y_{t-K+1}^t)$ is, by definition, the one step ahead prediction error (or *innovation sequence*) of $y(t)$ given its past. We therefore have: $p(y(t) | Y_{t-K+1}^t) = p(e(t) | Y_{t-K+1}^t)$. Where $e(t)$ is the optimal prediction error for each time t and is therefore independent on each time t .

Remark: In practice we do not know F^* and we use our predictor learnt from normal data as a proxy. This implies the prediction residuals are approximately independent on normal data (the predictor can explain data well), while the prediction residuals are, in general, correlated on abnormal data.

To summarize: under normal conditions the joint distribution of Y_c^t can be written as:

$$p(Y_c^t) = \prod_{i=c}^t p(y(i) | Y_c^{i-1}) = \prod_{i=c}^t p(e(i)) \quad (24)$$

in the normal conditions, and as:

$$p(Y_c^t) = \prod_{i=c}^t p(y(i) | Y_c^{i-1}) = \prod_{i=c}^t p(e(i) | E_c^{i-1}) \quad (25)$$

in the abnormal conditions.

These two conditions in turn influence the log likelihood ratio test as follows: under $H_0 \implies \prod_{i=c}^t \frac{p_a(e(i))}{p_n(e(i))}$ while under $H_c \implies \prod_{i=c}^t \frac{p_a(e(i)|E_c^{i-1})}{p_n(e(i))}$. The main issue here is the numerator under H_c : the distribution of residuals changes at each time-stamp (it is a conditional distribution) and $p_a(e(i) | E_c^{i-1})$ is difficult to approximate (it requires the model of the fault). In the following we show that replacing $p_a(e(i) | E_c^{i-1})$ with $p_a(e(i))$ allows us to compute a lower bound on the cumulative sum. Such an approximation is necessary to estimate the likelihood ratio in abnormal conditions, the main downside of this approximation is that the detector becomes slower (it needs more time to reach the stopping time threshold).

Applying the independent likelihood test in a correlated setting: We now show that treating $p_a(e(i) | E_c^{i-1})$ as independent random variables $p_a(e(i))$ for $i = 1, \dots, t$ allows us to compute a lower bound on the log likelihood $\log \Omega_c^t$ (i.e. the cumulative sum). We denote the cumulative sum of the log likelihood ratio using independent variables as $\log \bar{\Omega}_c^t = \sum_{i=c}^t \log \frac{p_a(e(i))}{p_n(e(i))}$

Proposition A.2 *Assume a change happens at time c so that H_c is true and the following log likelihood ratio holds true: $\log \Omega_c^t = \sum_{i=c}^t \log \frac{p_a(e(i)|E_c^{i-1})}{p_n(e(i))}$. Then it holds $\log \Omega_c^t \geq \log \bar{\Omega}_c^t$.*

Proof A.3 *By simple algebra we can write:*

$$\frac{p_a(e(i) | E_c^{i-1})}{p_n(e(i))} = \frac{p_a(e(i) | E_c^{i-1})}{p_a(e(i))} \frac{p_a(e(i))}{p_n(e(i))} \quad \forall i$$

Now recall the cumulative sum of the log-likelihood ratios taken under the current data generating mechanism $p_a(E_1^t)$ provides an estimate of the expected value of the log-likelihood ratio. Due to the correlated nature of data E_1^t the samples are drawn from a multidimensional distribution of dimension t (a sample from this distribution is an entire trajectory from c to t).

We now take the expectation of previous formula w.r.t. the ‘true’ distribution $p_a(E_1^t)$:

$$\begin{aligned}
\mathbb{E}_{p_a(E_c^t)} \Omega_c^t &= \mathbb{E}_{p_a(E_c^t)} \log \prod_{i=c}^t \frac{p_a(e(i) | E_c^{i-1})}{p_n(e(i))} \\
&= \mathbb{E}_{p_a(E_c^t)} \log \prod_{i=c}^t \frac{p_a(e(i) | E_c^{i-1})}{p_a(e(i))} \\
&\quad + \mathbb{E}_{p_a(E_c^t)} \log \prod_{i=c}^t \frac{p_a(e(i))}{p_n(e(i))} \\
&= MI\left(p_a(E_c^t); \prod_{i=c}^t p_a(e(i))\right) \\
&\quad + KL\left(\prod_{i=c}^t p_a(e(i)) \parallel \prod_{i=c}^t p_n(e(i))\right) \\
&\geq KL\left(\prod_{i=c}^t p_a(e(i)) \parallel \prod_{i=c}^t p_n(e(i))\right)
\end{aligned}$$

where we used the fact the mutual information is always non negative.

How to approximate pre and post fault distributions: Both p_n and p_a are not known and their likelihood ratio need to be estimated from available data. From Section 5.1.1 we know how to approximate the likelihood ratio given two set of data without estimating the densities. In our anomaly detection setup we define these two sets as: $E_n := E_{t-n_a-n_a+1}^{t-n_a}$ and $E_a := E_{t-n_a+1}^t$. So that given current time t we look back at a window of length $n_a + n_a$. The underlying assumption is that under H_c normal data are present in E_n and abnormal ones in E_a . We estimate the likelihood ratio $\frac{p_a(e(t))}{p_n(e(t))}$ at each time t by assuming both E_n and E_a data are independent (see Proposition A.2) and cumulate their log as t increases.

How do n_a and n_a affect our detector? The choice of the windows length (n_a and n_a) is fundamental and highly influences the likelihood estimator. Using small windows makes the detector highly sensible to both point and sequential outliers, while larger windows are better suited to estimate only sequential outliers. We now assume $n_a = n_a$ and study how small and large values affect the behaviour of our detector in simple working conditions.

In Figure 5 and Figure 6 we compute the cumulative sum of log likelihood ratios estimated from data on equally sized windows. Intuitively any local minimum after a ‘‘large’’ (depending on the threshold ϵ) increase of the cumulative sum is a candidate abnormal point.

In Figure 7 and Figure 8 we compare the cumulative sum of estimated likelihood ratios on data in which both sequential and point outliers are present. In particular we highlight that large window sizes n_a and n_a are usually not able to capture point anomalies Figure 7 while using small window sizes allow to detect both (at the expenses of a more sensitive detector) Figure 8.

A.6 DATASETS

A.6.1 CREDIT CARD

Credit card dataset ² is collected by openML, it contains credit cards transactions in September 2013 by European cardholders. The fraudulent transactions are labeled as outliers.

A.6.2 CICIDS

CICIDS dataset ³ is collected by Canadian Institute for Cybersecurity in 2017. We follow Lai et al. (2021) and adopt ‘‘Thursday-WorkingHours-Morning-WebAttacks’’ file in 2017 datasets which

²<https://www.openml.org/d/1597>

³<https://www.unb.ca/cic/datasets/ids-2017.html>

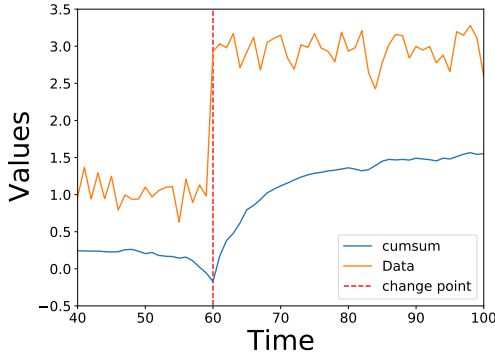


Figure 5: **Change point:** Cumulative sum (blue) obtained with our method in a synthetic example. We use the cumulative sum of estimated likelihood ratios on data in which a change point is present at $t = 60$. We use $n_a = n_a = 20$ and kernel length scale=0.2

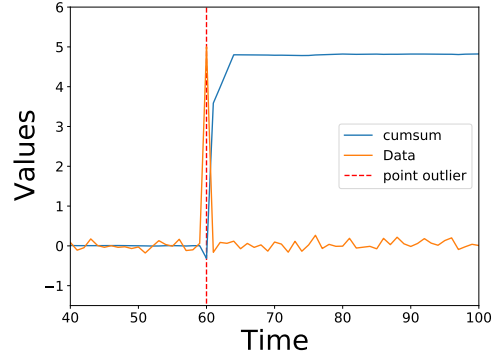


Figure 6: **Point anomaly:** Cumulative sum (blue) obtained with our method in a synthetic example. We use the cumulative sum of estimated likelihood ratios on data in which a point outlier is present at $t = 60$. We use $n_a = n_a = 2$ and kernel length scale=2.

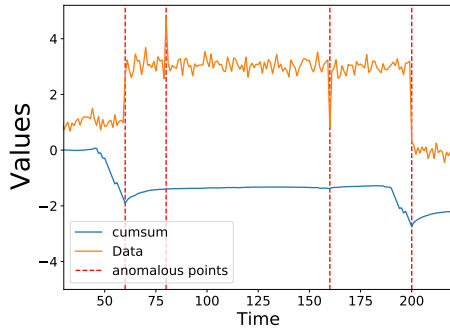


Figure 7: **Large n_a and n_a :** Cumulative sum (blue) obtained with our method in a synthetic example. We use the cumulative sum of estimated likelihood ratios on data which contain both change points ($t = 60$ and $t = 200$) and point outliers ($t = 80$ and $t = 160$). We use $n_a = n_a = 20$ and kernel length scale=1.

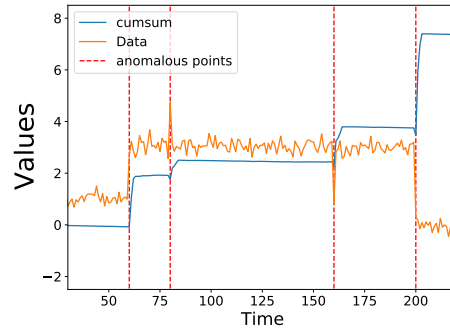


Figure 8: **Small n_a and n_a :** Cumulative sum (blue) obtained with our method in a synthetic example. We use the cumulative sum of estimated likelihood ratios on data which contain both change points ($t = 60$ and $t = 200$) and point outliers ($t = 80$ and $t = 160$). We use $n_a = n_a = 3$ and kernel length scale=5.

contains 3 kinds of intrusion attack: XSS, SQL injection and brute force attack. See Lai et al. (2021) for details on the pre-processing and data cleaning.

A.6.3 GECCO

GECCO dataset Lai et al. (2021) is collected by SPOTSeven Lab. This dataset describes an IoT for drinking water monitoring application and contains both point and pattern-wise outliers.

A.6.4 SWAN-SF

SWAN-SF dataset Lai et al. (2021) is collected by Harvard Dataverse, it describes an extreme space wather detection application. We follow Lai et al. (2021) pre-processing and data cleaning procedure. This dataset contains both point and pattern-wise outliers.

A.6.5 YAHOO DATASET

Yahoo Webscope dataset (Laptev & Amizadeh, 2020) is a publicly available dataset containing 367 real and synthetic time series with point anomalies, contextual anomalies and change points. Each time series contains 1420-1680 time stamps. This dataset is further divided into 4 sub-benchmarks: A1 Benchmark, A2 Benchmark, A3 Benchmark and A4 Benchmark. A1Benchmark is based on the real production traffic to some of the Yahoo! properties. The other 3 benchmarks are based on synthetic time series. A2 and A3 Benchmarks include point outliers, while the A4Benchmark includes change-point anomalies. All benchmarks have labelled anomalies. We use such information only during evaluation phase (since our method is completely unsupervised).

A.6.6 NAB DATASET

NAB (Numenta Anomaly Benchmark) (Lavin & Ahmad, 2015) is a publicly available anomaly detection benchmark. It consists of 58 data streams, each with 1,000 - 22000 instances. This dataset contains streaming data from different domains including read traffic, network utilization, on-line advertisement, and internet traffic. As done in (Geiger et al., 2020) we choose a subset of NAB benchmark, in particular we focus on the NAB Traffic and NAB Tweets benchmarks.

A.6.7 CO2 DATASET

We test the prediction and interpretability capabilities of our model on the CO2 dataset from kaggle⁴. The main goal here is to predict both trend and periodicity of CO2 emission rates on different years. Note this is not an Anomaly detection task.

Table 3: **Multivariate datasets summaries.** We report some properties of the datasets taken from Lai et al. (2021); Su et al. (2019); Abdulaal et al. (2021).

	TODS				Server application	
	Credit Card	CICIDS	GECCO	SWAN-SF	SMD	PSM
dimension	29	79	10	39	38	25
# Training					566,724	105,984
# Validation					141,681	26,497
# Test					708,420	87,841
# Tot data	284,807	170,231	138,521	120,000	1,416,825	220,322
% anomalies	0.173 %	1.281 %	1.246 %	23.8 %	4.2 %	27.8 %

Table 4: **Univariate datasets summaries.** We report some properties of the datasets used (see (Geiger et al., 2020) for mode details).

	Yahoo				NAB		Kaggle
	A1	A2	A3	A4	Traffic	Tweets	CO2
# signals	67	100	100	100	7	10	9
# anomalies	178	200	939	835	14	33	
point	68	33	935	833	0	0	
sequential	110	167	4	2	14	33	
# anomalous	1669	466	943	837	1560	15651	
points							
(% tot)	1.8%	0.32%	0.56%	0.5%	9.96%	9.87%	
# data points	94866	142100	168000	168000	15662	158511	4323

A.6.8 NYT DATASET

The New York Times Annotated Corpus⁵ (Sandhaus, 2008) contains over 1.8 million articles written and published by the New York Times between January 1, 1987 and June 19, 2007. We pre-processed the lead paragraph of each article with a pre-trained BERT model (Devlin et al., 2019) from the HuggingFace Transformers library (Wolf et al., 2020) and extracted the 768-dimensional

⁴<https://www.kaggle.com/txttrouble/carbon-emissions>

⁵<https://catalog.ldc.upenn.edu/LDC2008T19>

hidden state of the [CLS] token (which serves as an article-level embedding). For each day between January 1, 2000 and June 19, 2007, we took the mean of the embeddings of all articles from that day. Finally, we computed a PCA and kept the first 200 principal components (which explain approximately 95% of the variance), thus obtaining a 200-dimensional time series spanning 2727 consecutive days. Note that we did not use any of the dataset’s annotations, contrary to prior work such as Rayana & Akoglu (2015).

A.7 EXPERIMENTAL SETUP

In this section, we shall describe the experimental setup we used to test STRIC.

Data preprocessing: Before learning the predictor we standardize each dataset to have zero mean and standard deviation equals to one. As done in (Braei & Wagner, 2020) we note standardization is not equal to normalization, where data are forced to belong to the interval $(0, 1)$. Normalization is more sensitive to outliers, thus it would be inappropriate to normalize our datasets, which contain outliers.

We do not apply any deseasonalizing or detrending pre-processing.

Data splitting: We split each dataset into training and test sets preserving time ordering, so that the first data are used as train set and the following ones are used as test set. The data used to validate the model during optimization are last 10% of the training dataset. Depending on the experiment, we choose a different percentage in splitting train and test. When comparing with (Braei & Wagner, 2020) we used 30% as training data, while when comparing to (Munir et al., 2019) we use 40%. Such a choice is dictated by the particular (non uniform) experimental setup reported in (Braei & Wagner, 2020; Munir et al., 2019) and has been chosen to produce comparable results with state of the art methods present in literature. For SMD and PSM we maintain the standard train-validation-test split, see Table 3.

Evaluation metrics: We compare different predictors by means of the RMSE (root mean squared error) on the one-step ahead prediction errors. Given a sequence of data Y_1^N and the one-step ahead predictions \hat{Y}_1^N the RMSE is defined as: $\sqrt{\frac{1}{N} \sum_{i=1}^N \|y(i) - \hat{y}(i)\|^2}$.

As done in (Braei & Wagner, 2020) we compare different anomaly detection methods taking into account several metrics. We use F1-Score which is defined as the harmonic mean of Precision and Recall (see (Braei & Wagner, 2020; Munir et al., 2019)) and another metric that is often used is *receiver operating characteristic curve*, ROC-Curve, and its associated metric *area under the curve* (AUC). The AUC is defined as the area under the ROC-Curve. This metric is particularly useful in our anomaly detection setting since it describes with an unique number *true positive rate* and *false positive rate* on different threshold values. We now follow (Braei & Wagner, 2020) to describe how AUC is computed. Let the *true positive rate* and *false positive rate* be defined, respectively, as: $TPR = \frac{TP}{P}$ and $FPR = \frac{FP}{N}$, where TP stands for *true positive*, P for *positive*, FP for *false positive* and N for *negative*. To compute the ROC-Curve we use different thresholds on our anomaly detection method. We therefore have different pairs of TPR and FPR for each threshold. These values can be plotted on a plot whose x and y axes are, respectively: FPR and TPR . The resulting curve starts at the origin and ends in the point $(1,1)$. The AUC is the area under this curve. In anomaly detection, the AUC expresses the probability that the measured algorithm assigns a random anomalous point in the time series a higher anomaly score than a random normal point.

Hardware: We conduct our experiments on the following hardware setup:

- Processor: Intel(R) Core(TM) i9-10980XE CPU @ 3.00GHz
- RAM: 128 Gb
- GPU: Nvidia TITAN V 12Gb and RTX 24Gb

Hyper-parameters: All the experiments we carried out are uniform on the optimization hyper-parameters. In particular we fixed the maximum number of epochs to 300, the learning rate to 0.001 and batch size to 100. We optimize each model using Adam and early stopping.

We fix STRIC’s first module hyper-parameters as follows:

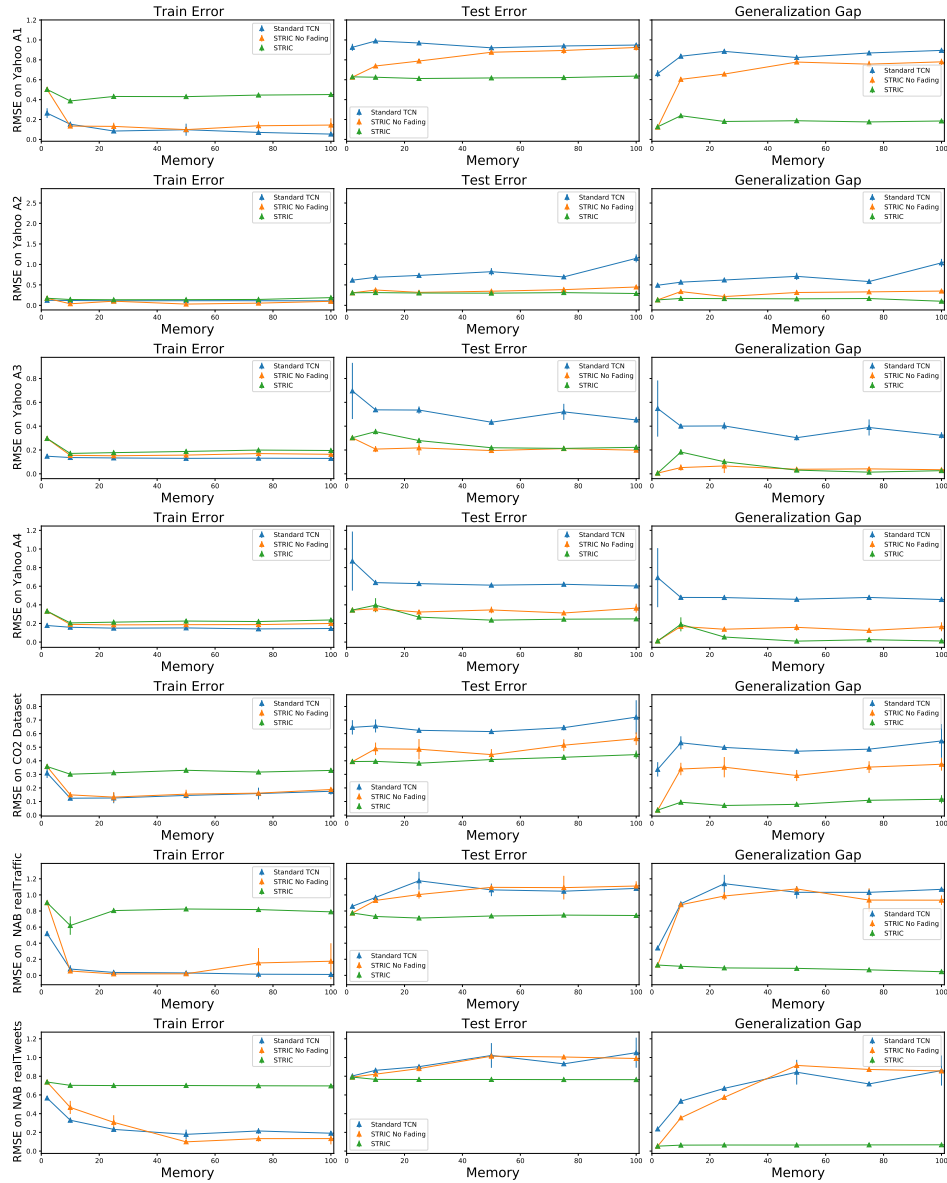


Figure 9: **Ablation studies on different datasets:** Effects of interpretable blocks and fading regularization on model’s forecasting as the available window of past data increases (memory). **Left Panel:** Train error. **Center Panel:** Test error. **Right Panel:** Generalization Gap. The test error of STRIC is uniformly smaller than a standard TCN (without interpretable blocks nor fading regularization). Adding interpretable blocks to a standard TCN improves generalization for fixed memory w.r.t. Standard TCN but get worse (overfitting occurs) as soon as the available past data horizon increase. Fading regularization is effective: STRIC generalization GAP is almost constant w.r.t. past horizon.

Table 5: **Comparison with SOTA anomaly detectors:** We compare STRIC with other anomaly detection methods (see Appendix A.9) on the experimental setup and the same evaluation metrics proposed in (Braei & Wagner, 2020; Munir et al., 2019; Lai et al., 2021). The baseline models are: ARIMA, OCSVM Lai et al. (2021), LSTM (Braei & Wagner, 2020; Munir et al., 2019), Omni-Anomaly (Su et al., 2019), TanoGAN (Bashar & Nayak, 2020), TadGAN (Geiger et al., 2020), and DeepAnT (Munir et al., 2019). STRIC outperforms most of the other methods based on statistical models and based on DNNs.

	F1	Yahoo A1	Yahoo A2	Yahoo A3	Yahoo A4	NAB Tweets	NAB Traffic
Models	ARIMA	0.35	0.83	0.88	0.70	0.57	0.57
	OCSVM	0.34	0.90	0.64	0.64	0.49	0.43
	LSTM	0.44	0.97	0.72	0.59		
	OmniAnomaly	0.47	0.95	0.80	0.64	0.69	0.70
	TanoGAN	0.41	0.86	0.59	0.63	0.54	0.51
	TadGAN	0.40	0.87	0.68	0.60	0.61	0.49
	DeepAnT	0.46	0.94	0.87	0.68		
	STRIC (ours)	0.48	0.98	0.89	0.68	0.71	0.73

Table 6: **Ablation study on the RMSE of prediction errors:** We compare Test error and Generalization Gap (Gap.) of a standard TCN model with our STRIC predictor and some variation of it (using the same training hyper-parameters). Standard deviations are given in Table 7.

	TCN		TCN + Linear		TCN + Fading		STRIC pred	
	Test	Gap.	Test	Gap.	Test	Gap.	Test	Gap.
	Datasets							
Yahoo A1	0.92	0.82	0.88	0.78	0.92	0.48	0.62	0.19
Yahoo A2	0.82	0.71	0.35	0.22	0.71	0.50	0.30	0.16
Yahoo A3	0.43	0.30	0.22	0.06	0.40	0.25	0.22	0.03
Yahoo A4	0.61	0.46	0.35	0.16	0.55	0.38	0.24	0.01
CO2 Dataset	0.62	0.48	0.45	0.30	0.61	0.43	0.41	0.08
NAB Traffic	1.06	1.03	1.00	0.96	0.93	0.31	0.74	0.11
NAB Tweets	1.02	0.84	0.98	0.78	0.83	0.36	0.77	0.07

- number of filter per block: $l_0 = 10, l_1 = 100, l_2 = 200$
- linear filters kernel lengths (N_0, N_1, N_2): half predictor’s memory

In all experiments we either use a TCN composed of 3 hidden layers with 300 nodes per layer or a TCN with 8 layers and 32 nodes per layer. Moreover we chose $N_3 = 5$ (TCN kernels’ lengths) and relu activation functions (Bai et al., 2018).

Comparison with SOTA methods: We tested our model against other SOTA methods (Table 1) in a comparable experimental setup. In particular, we chose comparable window lengths and architecture sizes (same order of magnitude of the number of parameters) to make the comparison as fair as possible. For classical anomaly detection methods we use hyper-parameters search used described in Appendix C of Lai et al. (2021). For the hyper-parameters details of any deep learning based SOTA method we use, we refer to the relative cited reference. We point out that while the window length is a critical hyper-parameter for the accuracy of many methods, our architecture is robust w.r.t. choice of window length: thanks to our fading regularization, the user is required only to choose a window length larger than the optimal one and then our automatic complexity selection is guaranteed to find the optimal model complexity given the available data Section 4.1.

Anomaly scores: When computing the F-score we use the predictions of the CUMSUM detector which we collect as a binary vector whose length is the same as the number of available data. Ones are associated to the presence of an anomalous time instants while zeros are associated to normality.

When computing the AUC we need to consider a continuous anomaly score, therefore the zero-one encoded vector from the CUMSUM is not usable. We compute the anomaly scores for each time instant as the estimated likelihood ratios. Since we write the likelihood ratio as $\frac{p_a}{p_n}$, it is large when data does not come from p_n (which we consider the reference distribution).

Table 7: **Ablation study on the RMSE of prediction errors with standard deviation on 10 different seeds:** We compare a standard TCN model with our STRIC predictor and some variation of it (using the same train hyper-parameters). The effect of adding a linear interpretable model before a TCN improves generalization error. Fading regularization has a beneficial effect in controlling the complexity of the TCN model and reducing the generalization gap.

	TCN		TCN + Linear		TCN + Fading		STRIC pred	
	Train	Test	Train	Test	Train	Test	Train	Test
	Datasets							
Yahoo A1	0.10 \pm 0.06	0.92 \pm 0.06	0.10 \pm 0.03	0.88 \pm 0.03	0.44 \pm 0.03	0.92 \pm 0.03	0.43 \pm 0.02	0.62 \pm 0.02
Yahoo A2	0.11 \pm 0.02	0.82 \pm 0.02	0.13 \pm 0.01	0.35 \pm 0.02	0.20 \pm 0.01	0.71 \pm 0.01	0.14 \pm 0.01	0.30 \pm 0.01
Yahoo A3	0.13 \pm 0.01	0.43 \pm 0.01	0.16 \pm 0.01	0.22 \pm 0.01	0.15 \pm 0.01	0.40 \pm 0.01	0.19 \pm 0.01	0.22 \pm 0.01
Yahoo A4	0.15 \pm 0.01	0.61 \pm 0.01	0.19 \pm 0.01	0.35 \pm 0.01	0.17 \pm 0.01	0.55 \pm 0.01	0.23 \pm 0.01	0.24 \pm 0.01
CO2 Dataset	0.14 \pm 0.02	0.62 \pm 0.02	0.15 \pm 0.02	0.45 \pm 0.02	0.18 \pm 0.03	0.61 \pm 0.03	0.33 \pm 0.01	0.41 \pm 0.01
NAB Traffic	0.03 \pm 0.01	1.06 \pm 0.02	0.04 \pm 0.01	1.00 \pm 0.02	0.62 \pm 0.01	0.93 \pm 0.01	0.63 \pm 0.02	0.74 \pm 0.02
NAB Tweets	0.18 \pm 0.05	1.02 \pm 0.05	0.20 \pm 0.05	0.98 \pm 0.05	0.47 \pm 0.02	0.83 \pm 0.02	0.70 \pm 0.01	0.77 \pm 0.01

A.8 ABLATION STUDY

In Figure 9 we show different metrics based on the predictor’s RMSE (training, test and generalization gap) as a function of the memory of the predictor. We test our fading regularization on a variety of different datasets. In all situations fading regularization helps improving test generalization and preserving the generalization gap (by keeping it constant) as the model complexity increases. All plots show confidence intervals around mean values evaluated on 10 different random seeds.

In Table 7 we extend the results by adding uncertainties (measured by standard deviations on 10 different random seeds) to the values of train and test RMSE on different ablations of STRIC. Despite the high variability across different datasets STRIC achieves the most consistent results (smaller standard deviations both on training and testing). In Table 2, we report the test RMSE prediction errors and the RMSE generalization gap (i.e. difference between test and training RMSE prediction errors) for different datasets while keeping all the training and models parameters the same (as done in the main text). The addition of the linear interpretable model before the TCN slightly improves the test error. We note this effect is more visible on A2, A3, A4, mainly due to the non-stationary nature of these datasets and the fact that TCNs do not easily approximate trends (Braei & Wagner, 2020) (we further tested this in Appendix A.8). While STRIC generalization is always better than a standard TCN model and STRIC’s ablated components, we note that applying Fading memory regularization alone to a standard TCN does not always improve generalization (but never decreases it): this highlights that the benefits of combining the linear module and the fading regularization together are not a trivial ‘sum of the parts’. Consider for example Yahoo A1: STRIC achieves 0.62 test error, the best ablated model (TCN + Linear) 0.88, while TCN + Fading does not improve over the baseline TCN. A similar observation holds for the CO2 Dataset. Fading regularization might not be beneficial (nor detrimental) for time series containing purely periodic components which correspond to infinite memory systems (systems with unitary fading coefficient). In such cases the interpretable module is essential in removing the periodicities and providing the regularized non-linear module (TCN + Fading) with an easier to model residual signal. We refer to Figure 4 (first column) for a closer look on a typical time series in CO2 dataset, which contains a periodic component that is captured by the seasonal part of the interpretable model. To conclude, our proposed fading regularization has (on average) a beneficial effect in controlling the complexity of a standard TCN model and reduces its generalization gap ($\approx 40\%$ reduction). Moreover, coupling fading regularization with the interpretable module guarantees the best generalization.

Finally, in Table 8 we show the effects on different choices of the predictor’s memory n_{pred} and length of the anomaly detectors windows n_{det} on the detection performance of STRIC. Note both F-score and AUC are highly sensible to the choice of n_{det} : the best results are achieved for small windows. On the other hand when n_{det} is large the performance drops. This is due to the type of anomalies present in the Yahoo benchmark: most of them can be considered to be point anomalies. In fact, as we showed in Appendix A.5, our detector is less sensible to point anomalies when a large window n_{det} is chosen.

In Table 8 we also report the reconstruction error of the optimal predictor given its memory n_{pred} . Note small memory in the predictor introduce modelling bias (higher training error) while a large memory does not (thanks to fading regularization). As we observed in Appendix A.5 better predictive models provide the detection module with more discriminative residuals: the downstream detection module achieves better F-scores and AUC.

Table 8: **Sensitivity of STRIC to hyper-parameters:** We compare STRIC on different anomaly detection benchmarks datasets using different hyper-parameters: memory of the predictor n_{pred} and length of anomaly detector windows $n_p = n_f = n_{\text{det}}$.

		Yahoo A1		Yahoo A2		Yahoo A3		Yahoo A4	
		F1	AUC	F1	AUC	F1	AUC	F1	AUC
Models	$n_{\text{pred}} = 10, n_{\text{det}} = 2$	0.45	0.89	0.63	0.99	0.87	0.99	0.64	0.89
	$n_{\text{pred}} = 100, n_{\text{det}} = 2$	0.48	0.9308	0.98	0.9999	0.99	0.9999	0.68	0.9348
	$n_{\text{pred}} = 10, n_{\text{det}} = 20$	0.10	0.58	0.63	0.99	0.47	0.83	0.37	0.72
	$n_{\text{pred}} = 100, n_{\text{det}} = 20$	0.10	0.55	0.98	0.9999	0.49	0.86	0.35	0.76
		Yahoo A1		Yahoo A2		Yahoo A3		Yahoo A4	
		Train	Test	Train	Test	Train	Test	Train	Test
Models	$n_{\text{pred}} = 10$	0.44	0.62	0.16	0.31	0.22	0.23	0.25	0.26
	$n_{\text{pred}} = 100$	0.42	0.61	0.14	0.30	0.19	0.22	0.23	0.24

A.8.1 COMPARISON TCN VS STRIC

In this section we show standard non-linear TCN without regularization and proper inductive bias might not generalize on non-stationary time series (e.g. time series with non zero trend component) and TCN architecture. In Figure 10 we compare the prediction errors of a standard TCN model against our STRIC on some simple time series in the A3 Yahoo dataset (the signal is the sum of a sinusoidal and a trend component). We train both models using the same optimization hyper-parameters as described in previous section. Note a plain TCN does not necessarily capture the trend component in the test set.

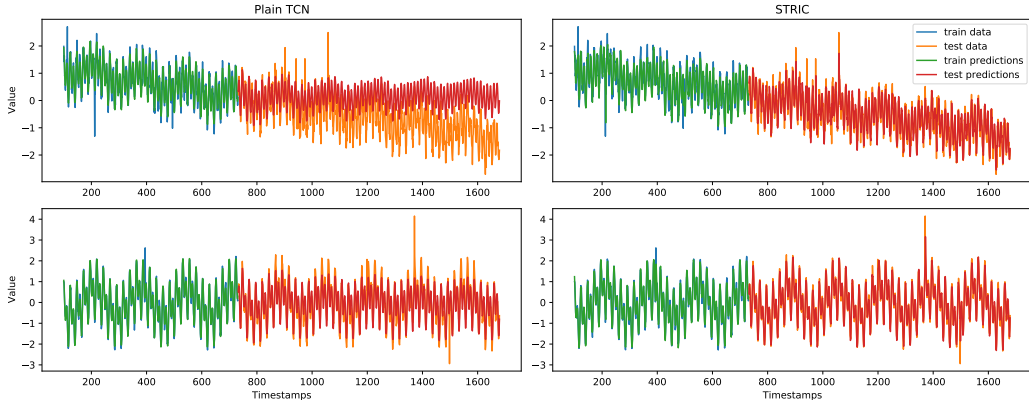


Figure 10: We compare an off-the-shelf TCN against STRIC (time series predictor) on the Yahoo dataset A3 Benchmark. Note the standard TCN overfits compared to STRIC: the standard TCN does not handle correctly the trend component of the signal (**First row**). If we consider a time series without trend, the standard TCN model performs better but overfitting is still present. In particular the generalization gap (measured using squared reconstruction error) for the two models is: Standard TCN 0.3735 and STRIC 0.0135.

A.9 STRIC VS SOTA ANOMALY DETECTORS

In this section we further expand the discussion on the main differences between STRIC and other SOTA anomaly detectors by commenting results obtained in Table 1. Both for F1 and AUC we report the following for each comparing SOTA method: $\frac{AUC_{\text{method}} - AUC_{\text{STRIC}}}{1 - AUC_{\text{STRIC}}} \cdot 100$ (similarly for F1).

Comparison with classic anomaly detection methods To begin with, STRIC outperforms ‘traditional’ methods (LOF and One-class SVM) which are considered as baselines models for comparing time series anomaly detectors. Interestingly, STRIC does not achieve the optimal F1 compared to linear models on Yahoo A4. The ability of linear models to outperform non-linear ones on Yahoo

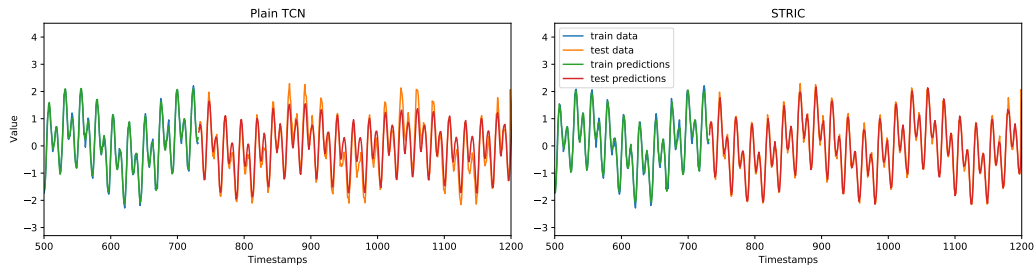


Figure 11: Zoom on the second row of panels in Figure 10. We show the interface between train and test data both on a plain TCN and on our STRIC predictor. A plain TCN overfits w.r.t. STRIC also when not trend is present.

A4 is known in the literature (e.g. in Geiger et al. (2020) any non-linear model is outperformed by AR/MA models of the proper complexity). The main motivation for this is that modern (non-linear) methods tend to overfit on Yahoo A4 and therefore generalization is usually low. Instead, thanks to fading regularization and model architecture, STRIC does not exhibit overfitting despite having larger complexity than SOTA linear models used in A4. To conclude, we believe that STRIC merges both the advantages of simple and interpretable linear models and the flexibility of non-linear ones while discounting their major drawbacks: lack of flexibility of linear models and lack of interpretability and overfitting of non-linear ones (see Appendix A.9 for a more in depth discussion).

Comparison with other Deep Learning based methods: STRIC outperforms most of the SOTA Deep Learning based methods reported in Table 1: TadGAN, TAnoGAN, DeepAnT and DeepAR (the last one is a SOTA time series predictor). Note the relative improvement of STRIC is higher on the Yahoo dataset where statistical models outperforms deep learning based ones. We believe this is due to both fading regularization and the seasonal-trend decomposition performed by STRIC.

Despite the general applicability of GOAD (Bergman & Hoshen, 2020) this method has not been designed to handle time series, but images and tabular data. “Geometric” transformations which have been considered in GOAD and actually have inspired it (rotations, reflections, translations) might not be straightforwardly applied to time series. Nevertheless, while we have not been able to find in the literature any direct and principled extension of this work to the time series domain, we have implemented and compared against (Bergman & Hoshen, 2020) by extending the main design ideas of GOAD to time-series. So that we applied their method on lagged windows extracted from time series (exploiting the same architectures proposed for tabular data case with some minor modifications). We report the results we obtained by running the GOAD’s official code on all our benchmark datasets. Overall, STRIC performs (on average) 70% better than GOAD on the Yahoo dataset and 15% better on the NAB dataset.

A.9.1 DETAILS ON THE NYT EXPERIMENT

We qualitatively test STRIC on a time series consisting of BERT embeddings (Devlin et al., 2019) of New York Times articles (Sandhaus, 2008) from 2000 to 2007. We set $n_a = n_p = 30$ days, to be able to detect change-point anomalies that altered the normal distribution of news articles for a prolonged period of time. Without any human annotation, STRIC is able to detect major historical events such as the 9/11 attack, the 2004 Indian Ocean tsunami, and U.S. elections (Figure 12). Note that we do not carry out a quantitative analysis of STRIC’s predictions, as we are not aware of any ground truth or metrics for this benchmark, see for example Rayana & Akoglu (2015). Additional details and comparison with a baseline model built on PCA are given in Appendix A.9.1.

Figure 12 shows the normalized anomaly score computed by STRIC on the NYT dataset, following the setup described in Appendix A.6.8. Some additional insights can be gained by zooming in around some of the detected change-points. In Figure 13 (left), we see that the anomaly score (blue line) rapidly increases immediately after the 9/11 attack and reaches its peak some days later. Such delay is inherently tied to our choice of time scale, that privileges the detection of prolonged anomalies as opposed to single-day anomalies (which are not meaningful due to the high variability of the news content). The change-point which occurs the day after the 9/11 attack is reflected by a sudden

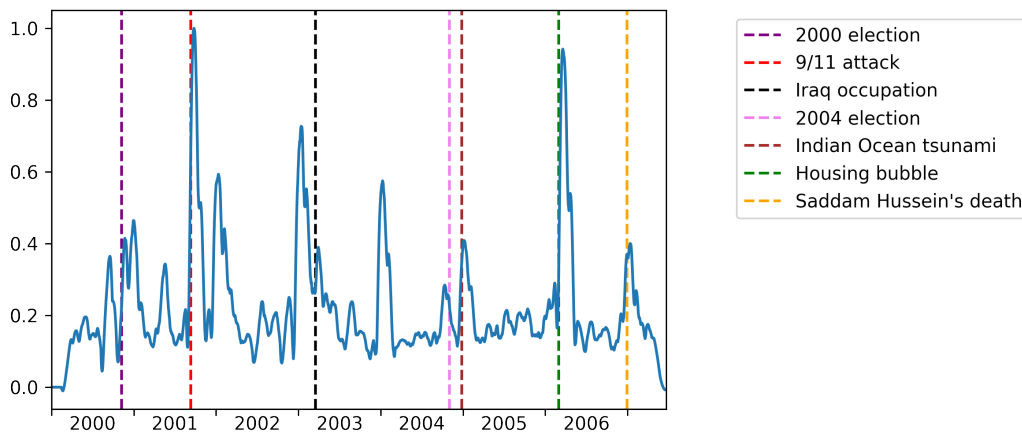


Figure 12: **Anomaly score on the New York Times dataset.** Our method finds anomalies in a complex time series consisting of the BERT embedding of articles from the New York Times. Peaks in the anomaly score correspond to historical events that sensibly changed the content of the news cycle.

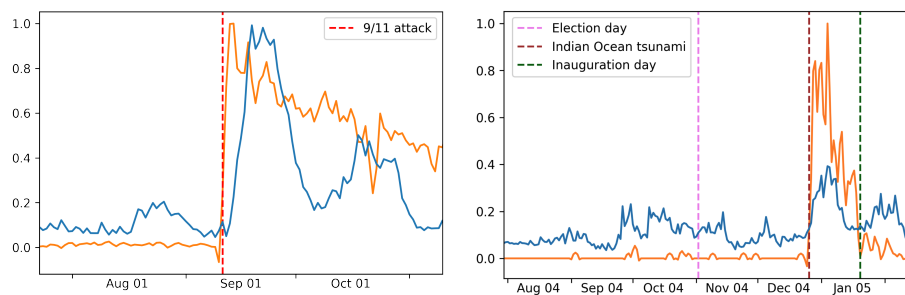


Figure 13: A closer look at some of the change-points detected by STRIC. **Left:** Normalized anomaly score (blue line) and normalized frequency of the “Terrorism” descriptor (orange line) around the 9/11 attack. **Right:** Normalized anomaly score (blue line) and normalized frequency of the “Earthquakes” descriptor (orange line) in the second half of 2004 and beginning of 2005. The 2004 U.S. election causes an increase in the anomaly score, but the most significant change-point occurs after the Indian Ocean tsunami.

increase of the relative frequency of article descriptors such as “Terrorism” (orange line). Article descriptors are annotated in the NYT dataset, but they are not given as input to STRIC so that we do not rely on any human annotations. However, they can help interpreting the change-points found by STRIC.

In Figure 13 (right), we can observe that the anomaly score (blue line) is higher in the months around the 2004 U.S. election and immediately after the inauguration day. However, the highest values for the anomaly score occur around the end of 2004, shortly after the Indian Ocean tsunami. Indeed, this is reflected by an abrupt increase of the frequency of descriptors like “Earthquakes” (orange line) and “Tsunami”.

We note this experiment is qualitative and unfortunately we are not aware of any ground truth or metrics (e.g., in Rayana & Akoglu (2015) a similar qualitative result has been reported on the NYT dataset). We therefore tested STRIC against a simple baseline which uses PCA on BERT features and a threshold to detect anomalies. Despite being a simple baseline, this method proved to be highly applied in practice due to its simplicity (Blázquez-García et al., 2020). The PCA + threshold baseline is able to pick up some events (2000 election, 9/11 attack, housing bubble) but is otherwise more noisy than STRIC’s anomaly score. This is likely due to the lack of a modeling of seasonal/periodic components. For instance, the anomaly score of the simple baseline contains many

false alarms which are related to normal weekly periodicity that is not easily modeled by the baseline. This does not affect STRIC's predictions, since normal weekly periodicity is directly modeled and identified as normal behaviour.